iScience

CellPress
OPEN ACCESS

Article

PD-L1 Expression Affects Neoantigen Presentation

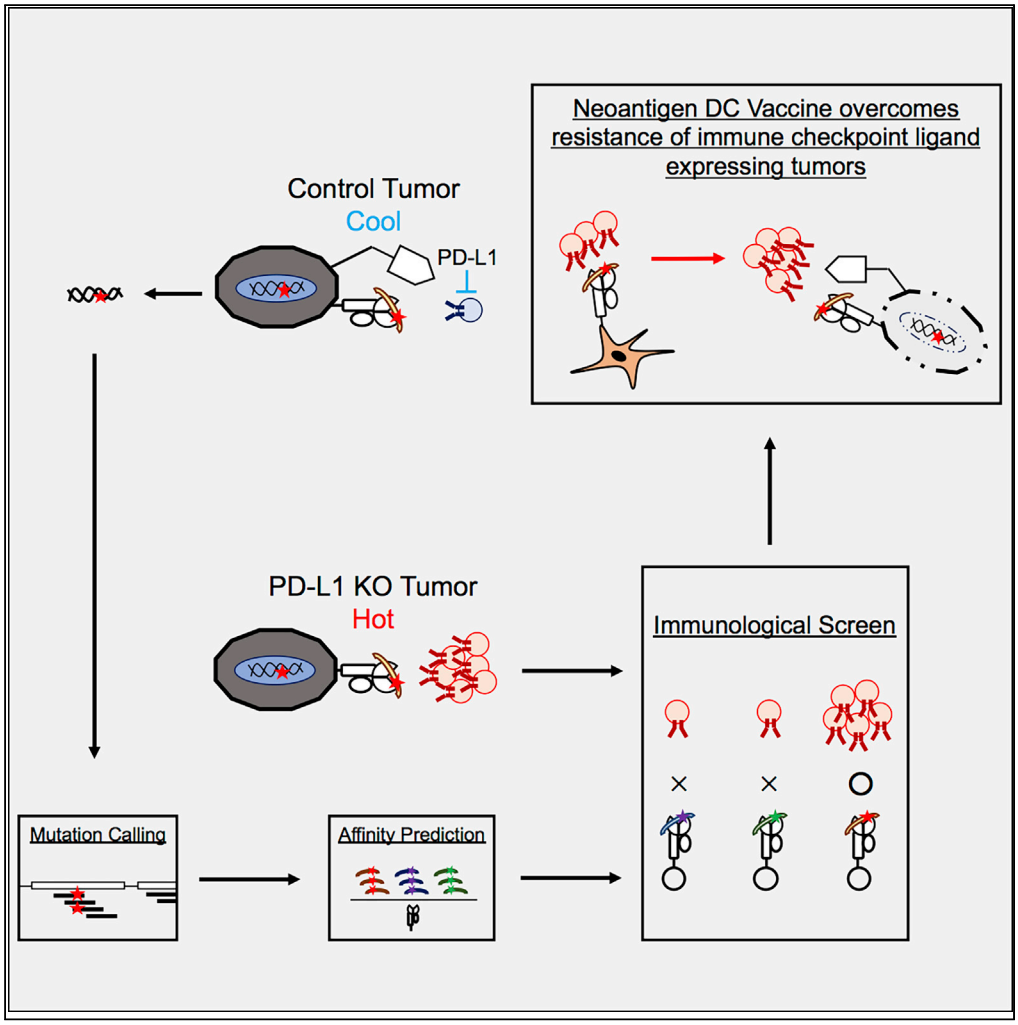

Masahiro Okada, Kanako Shimizu, Tomonori Iyoda, ..., Takashi Watanabe, Osamu Ohara, Shin-ichiro Fujii

shin-ichiro.fujii@riken.jp

HIGHLIGHTS

Poor prognosis of PD-L1-expressing tumors in some cancers

Identification of TCRVα and Vβ repertoire responsive for H2-K^{b}-restricted neoantigens

Neoantigen-epitope-pulsed DC therapy demonstrates antitumor effect in vaccine

Okada et al., iScience *23*, 101238
June 26, 2020 © 2020
https://doi.org/10.1016/j.isci.2020.101238

iScience

CellPress
OPEN ACCESS

Article

PD-L1 Expression Affects Neoantigen Presentation

Masahiro Okada,[1] Kanako Shimizu,[1] Tomonori Iyoda,[1] Shogo Ueda,[1] Jun Shinga,[1] Yoshiki Mochizuki,[2] Takashi Watanabe,[2] Osamu Ohara,[2] and Shin-ichiro Fujii[1,3,4,*]

SUMMARY

Although PD-L1 expression on tumor is related to the prognosis of immune checkpoint blockade (ICB) therapy, a recent study also demonstrated clinical benefits even in patients without PD-L1 expression. To understand the relationship between innate resistance and antitumor cytotoxic T lymphocyte (CTL) responses especially against neoantigens, the interaction between PD-L1$^+$ or genetically PD-L1-deleted colorectal tumors and CTLs was assessed under an ICB therapy, finding the robust CTL activation in PD-L1-deleted tumor-bearing mice. Using antigen libraries based on immunogenomics, we identified three H2-K^b-restricted, somatic-mutated immunogenic neoantigens by utilizing enhanced CTLs responses due to PD-L1 deficiency. Furthermore, we identified three T cell receptor (TCR) repertoires relevant to the neoantigens, confirming the response of TCR-gene-transduced CTLs to parental tumor cells. Notably, neoantigen-pulsed dendritic cell (DC) therapy reversed the tumor tolerance. Thus, innate resistance of tumors determines their responsiveness to neoantigens and mixed neoantigen peptides may be useful in DC therapy against innate resistance type tumor.

INTRODUCTION

Cancer immunotherapy has recently evolved into one of the most promising cancer treatment modalities. Although tumor cells hijack the immune system, in particular causing T cell exhaustion, several reports have demonstrated its reversal through immune checkpoint blockade (ICB), i.e., antibodies targeting cytotoxic T-lymphocyte-associated protein 4 (CTLA-4) and programmed cell death protein 1 (PD-1) (Hodi et al., 2016; Shimizu et al., 2018; Wei et al., 2018). Currently, these have been used as effective immunotherapeutic drugs. Specifically, ICB therapy has demonstrated improved overall survival (OS) and progression-free survival (PFS) in the treatment of many different tumor types, such as melanoma (Robert et al., 2015), non-small-cell lung cancer (NSCLC) (Brahmer et al., 2015), head and neck cancer (Ferris et al., 2016), and other cancers, due to the durable antitumor CD8$^+$ cytotoxic T lymphocytes (CTLs). In addition, ICB-therapy-induced recruitment of T cells in the tumor increases in hot tumors, but not in cold tumors (Tumeh et al., 2014; Topalian et al., 2016). Despite its successful clinical activity, still limited patients received the clinical benefits, for which many studies have addressed the factors related to ICB sensitivity and resistance.

The interplay between PD-1 and PD-L1 regulates T cells in the tumor microenvironment (TME). PD-1 expression is upregulated in activated T cells and remains high in exhausted T cells from tumor-infiltrating lymphocytes (Ahmadzadeh et al., 2009). Constitutive PD-L1 expression caused by aberrant transactivation due to genetic or signaling alteration in an intrinsic manner defines the innate resistance. After exposure to IFN-γ released by effector T cells, PD-L1 and other inhibitory molecules were induced at the transcription level and triggers the adaptive resistance (Topalian et al., 2015). Clinically, PD-L1 expression on tumors or immune cells in the tumor microenvironment is associated with durable clinical responses to anti-PD-1/PD-L1 therapies in many tumor types (Topalian et al., 2012; Herbst et al., 2014). However, the significance of PD-L1 expression in each cell type is controversial. PD-L1 expression on tumors or immune cells can independently attenuate antitumor T cell immunity. PD-1$^+$ T cells in the tumor are impaired due to interactions with PD-L1 expressed on either tumor cells (Juneja et al., 2017) or other tumor-infiltrating immune cells (e.g., myeloid cells or TAM) (Lin et al., 2018; Tang et al., 2018) in the TME. Furthermore, immune checkpoint knockout mice or wild-type (WT) mice treated with anti-PD-1 antibodies (Abs) suppressed tumor cells, indicating that the anti-PD-1 Ab has an antitumor effect on both PD-L1-expressing host tumor-associated

[1]Laboratory for Immunotherapy, RIKEN Center for Integrative Medical Sciences (IMS), Yokohama, Kanagawa 230-0045, Japan

[2]Laboratory for Integrative Genomics, RIKEN Center for Integrative Medical Sciences (IMS), Yokohama, Kanagawa 230-0045, Japan

[3]RIKEN Program for Drug Discovery and Medical Technology Platform (DMP), Yokohama, Kanagawa 230-0045, Japan

[4]Lead Contact

*Correspondence: shin-ichiro.fujii@riken.jp

https://doi.org/10.1016/j.isci.2020.101238

macrophages (TAM) and tumor cells (Kleffel et al., 2015; Lin et al., 2018). Recently, the functional importance of immune cells relative to the tumor has been reported in the regulation of the antitumor T cell response in NSCLC patients (Kowanetz et al., 2018), but its importance on the tumor still has to be evaluated. Furthermore, despite low PD-L1 expression on tumor, recent several reports demonstrated that some patients respond well to PD-1 pathway blockade (Brahmer et al., 2015; Zou et al., 2016; Rittmeyer et al., 2017; Eggermont et al., 2018), indicating that the relation of PD-L1 expression and ICB sensitivity partly depends on pathological conditions, thus ascribing PD-L1 expression to innate or acquired resistance. To elucidate the underlying mechanisms of these phenomena, CTL responses in the presence or absence of ICB treatment, with focus on PD-L1 expression on tumor cells should be compared.

The underlying genomic features of tumor cells contribute to ICB responses, and increased tumor mutation burden has been shown to be associated with survival benefits from both anti-CTLA-4 and anti-PD-1 therapy in multiple malignancies (Snyder et al., 2014; Le et al., 2015; Rizvi et al., 2015; Hugo et al., 2016). High mutation burden was frequently diagnosed in mutagen-associated cancers, such as melanoma and NSCLC as well as cancers associated with DNA-mismatch repair gene defects, such as microsatellite instability in colorectal cancers (Schumacher and Schreiber, 2015; Riaz et al., 2016). These high mutation burden tumors potentially generate immunogenic neoantigens. In fact, tumors with clonal neoantigens may significantly elicit effective immune responses (McGranahan et al., 2016), and peptides containing these mutations presented on MHC class I (MHC-I) can be recognized as "non-self" by T cells. For this purpose, neoantigens in high mutation burden tumors can be identified by whole-exome sequence and RNA sequence (RNA-Seq), and accompanying bioinformatics approaches can predict specific neoepitopes in individual cancers using MHC-I-binding algorithms and immunogenomics methods (Castle et al., 2012; Karasaki et al., 2017). Furthermore, ICB immunotherapy has sometimes been found to be effective even in cancer with a low number of mutations but containing some indels, such as renal cell carcinoma, indicating that the number of mutations present in tumors does not solely determine ICB responsiveness (Turajlic et al., 2017; Motzer et al., 2018; Yang et al., 2019). Based on these reports, there are many possible implications regarding ICB sensitive and resistant cases, particularly their PD-L1 expressions and potential neoantigen responses under ICB therapy. Nonetheless, comprehensive analyses are yet to be performed.

Development of a therapeutic strategy for ICB-resistant cancers is an important issue. Of which, dendritic cell (DC) vaccine was identified as a candidate, which plays a central role in linking innate and adaptive immune system responses (Fujii et al., 2004, 2007; Steinman, 2012; Bottcher and Reis, 2018; Fujii and Shimizu, 2019). *Ex vivo*-expanded DCs pulsed with MHC-I-restricted cancer testis antigen peptides (Bezu et al., 2018) and DCs electroporated with transfected mRNA coding tumor antigen (Bol et al., 2015) and tumor lysates or irradiated tumor cells (Fujii et al., 1999; Rojas-Sepulveda et al., 2018; Tanyi et al., 2018) have been demonstrated in many basic and clinical studies (Steinman and Banchereau, 2007; Saxena et al., 2018). It is noteworthy that utilizing neoantigens, several reports applied DC vaccines in clinical study and showed that neoantigen-pulsed DC can induce tumor regression through neoantigen-specific T cell responses in refractory solid tumors such as melanoma (Carreno et al., 2015; Chen et al., 2019).

Regarding PD-L1 expression in ICB treatment, PD-L1-mediated immune suppression by IFN-γ-induced adaptive resistance in T cell infiltrating hot tumors has been described (Spranger et al., 2013; Tumeh et al., 2014; Wilky, 2019). In contrast, the mechanism of PD-L1-mediated immune suppression by the tumor in a cell intrinsic manner, i.e., innate resistance, and its reversal by ICB therapy remain to be fully resolved. Furthermore, little is known about whether PD-L1 expression on tumors controls T cell immunity against neoantigens, which can partly determine the ICB response. Therefore, in the current study, we used several models—PD-L1-expressing or PD-L1-deleted tumor cells, with or without ICB (anti-PD-1 Ab and anti-CTLA-4 Ab) therapy—to explore how PD-L1 expression on tumor cells leads to innate resistance to ICB therapy and also elucidated potential mechanism of PD-L1-deleted tumor responses in ICB therapy. Further, we demonstrated the availability of our identified neoantigens-based DC therapy to compensate for ICB resistance, resulting in the generation of neoantigens responding T cell immunity as well as enhanced pre-existing immunity. Therefore, DCs vaccination has potential application for resistant tumors.

RESULTS

TCGA Analysis Indicates the Association between PD-L1 and Survival in Cancer Patients

PD-L1 expression in tumor sites is generally known to be associated with overall survival but differs in patients and their contexts. To clarify the variable association of PD-L1 expression and overall survival, we first

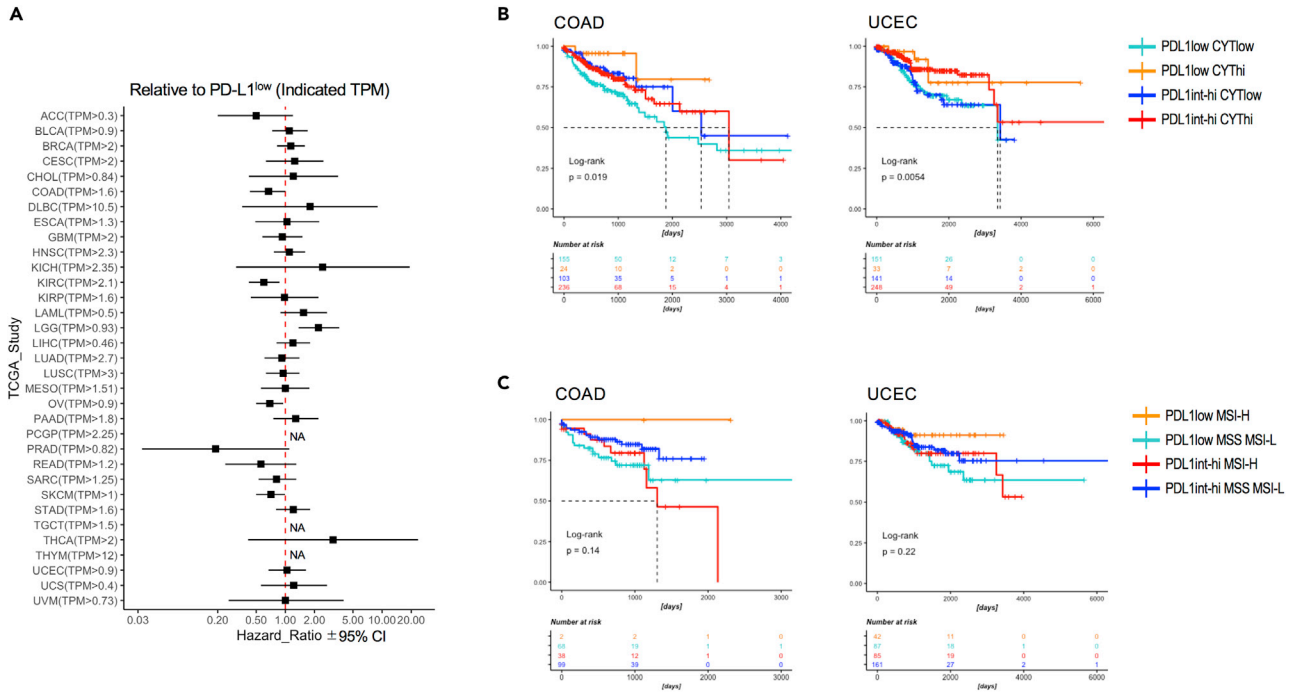

Figure 1. The Association between PD-L1 Expression in Tumor Tissue and Survival

(A) Forest plot of hazard ratios and 95% confidence intervals associated with PD-L1 expression. PD-L1 low expression groups in each study were referenced. NA, not analyzed due to low hazard ratios.

(B and C) Analysis of the association between PD-L1 expression and patient survival across TCGA colon cancer (left) and uterine corpus endometrial carcinoma (right). (B) Kaplan-Meier survival curves (time is measured on the x axis) of patients with high versus low CYT score. Log rank statistics: COAD, p = 0.019; UCEC, p = 0.0054. (C) Kaplan-Meier survival curves of patients with high versus low MSI. Data were analyzed by log rank statistics: COAD, p = 0.14; UCEC, p = 0.22.

analyzed all study cohorts in publicly available TCGA database (The Cancer Genome Atlas; Cancer Genome Atlas Research Network, 2014). PD-L1 expression in some cancers were related to better prognosis but varied among study (Figure 1A). Because the cytolytic score (CYT), that is, the level of granzyme A and perforin, was previously reported to be mainly associated with antitumor immunological effects (Rooney et al., 2015; Roufas et al., 2018), we sub-grouped based on PD-L1 expression, CYT score, and estimated survival. We found that PD-L1 low expression on hot tumors (CYT high) remarkably correlated with better prognosis, than the other three groups—PD-L1 low expression on the cold tumor (CYT low) or PD-L1 high expression—in colorectal adenocarcinoma (COAD) and uterine corpus endometrial carcinoma (UCEC) (Figure 1B). Some other cancers (breast invasive carcinoma [BRCA], cervical squamous cell carcinoma [CESC], diffuse large B cell lymphoma [DLBC], acute myeloid leukemia [LAML], liver hepatocellular carcinoma [LIHC], and sarcoma [SARC]), but not all, also show similar tendencies (Figure S1). In addition to previous observations of survival in patients with high microsatellite instability (MSI) (Gryfe et al., 2000; Le et al., 2015), a group of cancer patients with low PD-L1 expression and high MSI were also associated with better prognosis in these COAD and UCEC studies (Figure 1C). Thus, our results indicated that low PD-L1 expression with strong antitumor immunity or with potential mutation load is related to survival benefits in patients with certain tumors.

Anti-tumor CTL Responses in PD-L1^{+} or PD-L1-KO Tumors

In accordance with clinical observation, several murine tumors have been characterized, including B16 melanoma showing low PD-L1 expression and low immunogenicity with low T cell infiltration (known as a cold tumor type) and a murine colorectal MC38 expressing high PD-L1 and high immunogenicity with high T cell infiltration (known as a hot tumor type). In this study, MC38, which is known to be highly immunogenic and relatively responds to ICB treatment, was used to compare PD-L1 expression and T cell responses in ICB therapy(Yadav et al., 2014; Tanegashima et al., 2019). To examine an effect of PD-L1 of tumor cells on the antitumor immunity, we first generated genetically PD-L1-deleted tumors (hereafter MC38-PD-L1-KO cells)

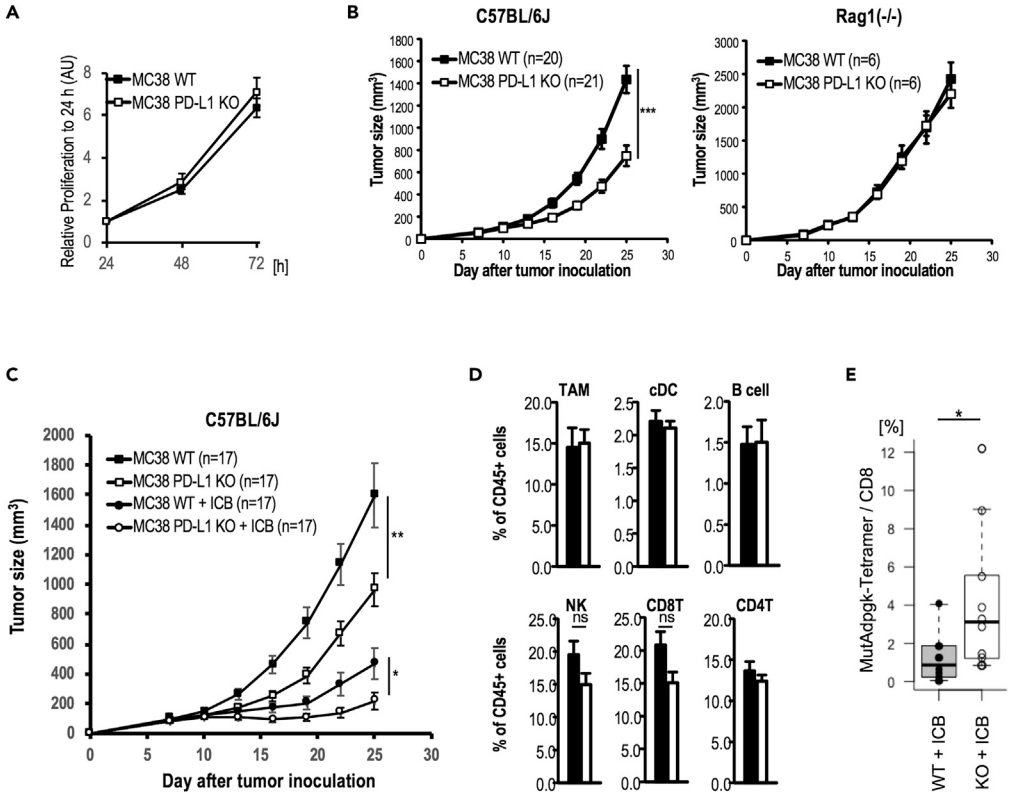

Figure 2. Enhanced Immune Responses of CTLs from PD-L1-KO Tumor

(A) Proliferating activity of MC38 or MC38-PD-L1-KO cells *in vitro* by WST-1 assay. Data are pooled from three independent experiments, and the values represent mean ± SD.

(B) C57BL/6J (left) or Rag1$^{-/-}$ (right) mice were injected with 5 × 10^5 MC38 or MC38-PD-L1-KO cells, subcutaneously (s.c.). Tumor growth was monitored at indicated time points by measuring three perpendicular diameters. MC38 or MC38-PD-L1-KO in C57BL/6J mice n = 20 and 21/group, respectively, in Rag1$^{-/-}$ mice, n = 6/group. Data are pooled from four and two independent experiments, and the values represent mean ± SEM.

(C) C57BL/6J mice were injected with 5 x 10^5 MC38 cells or MC38-PD-L1-KO cells s.c. and then treated with anti-PD-1 and anti-CTLA-4 on day 7, 10, and 13. Tumor growth was monitored at indicated time points by measuring three perpendicular diameters. (n = 17/group). Data are pooled from six independent experiments, and the values represent mean ± SEM.

(D) The frequency of immune cells in tumor sites was analyzed at day 15 after tumor inoculation by flow cytometric analysis. The values represent mean ± SD (n = 4/group). Closed and open bar indicated MC38 and MC38-PD-L1-KO tumor-bearing mice, respectively; ns indicates not significant.

(E) Tumor antigen-specific T cell response in ICB-treated MC38 or MC38-PD-L1-KO tumor-bearing mice. Frequency of MutAdpgk tetramer$^+$ in CD8$^+$ T cells was plotted. Data are pooled from four independent experiments; n = 10/group. Data were analyzed by unpaired Student's t test, *p < 0.05, **p < 0.01, ***p < 0.001.

by plasmid transfection-based transient CRISPR-Cas9 expression in the MC38 cell line. MC38-PD-L1-KO cells expressed MHC-I, but not PD-L1 (Figure S2A). We then examined the tumor proliferation activity *in vitro* and *in vivo*. There was no difference in the proliferation of tumor cells between MC38 and MC38-PD-L1-KO in an *in vitro* culture (Figure 2A). Subsequently, we compared tumor growth after a subcutaneous injection of MC38 and MC38-PD-L1-KO and found that tumor growth of MC38-PD-L1-KO was more slowly progressive than MC38 in WT mice, but not in Rag1$^{-/-}$ mice (Figure 2B), indicating T cell dependence. We also established the PD-L1-deficient murine breast cancer cell line, E0771, and confirmed similar phenomena (Figure S2B), but were not found with B16F10, probably due to the cold tumor type (Figure S2C). These imply that PD-L1 expression and tumor antigen presentation in tumor cells directly dampened the T-cell-dependent tumor suppression. Further, anti-PD-1 Ab treatment alone showed an antitumor effect by reactivating T cells in the tumor, although somewhat insufficient (Figure S2D). The combination of anti-PD-1 Ab plus anti-CTLA-4 Ab has been shown to be more promising for effective CTL generation (Hodi et al., 2016; Shimizu et al., 2018; Wei et al., 2018). To understand the relationship between CTL

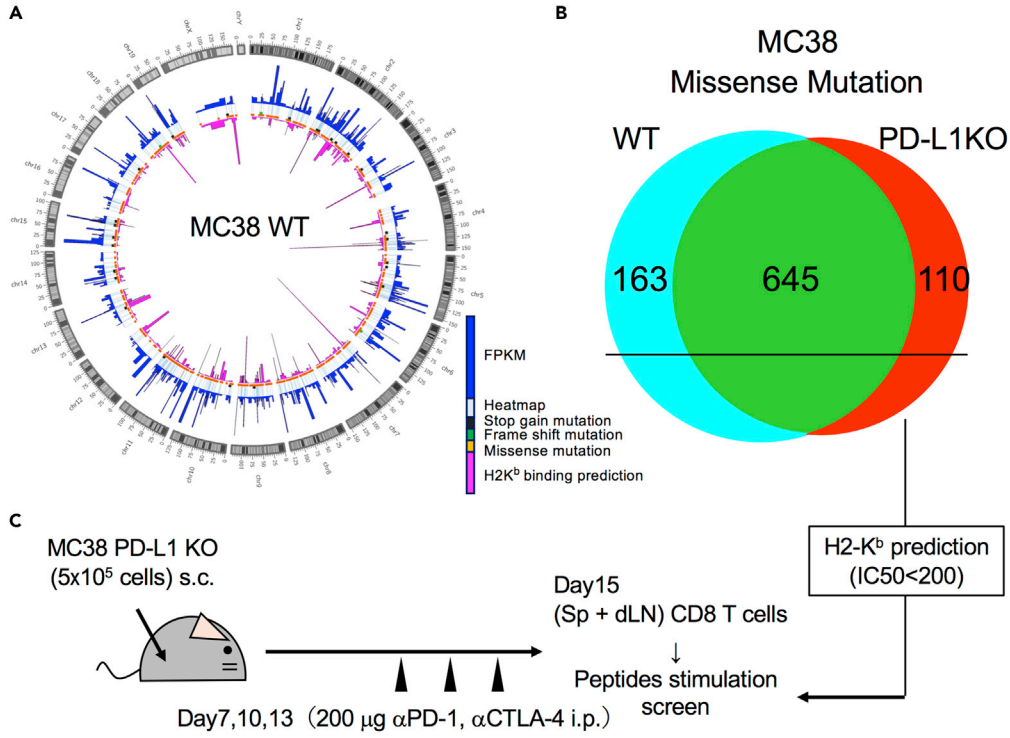

Peptide No #	Gene	Mutation Base/Amino Acid	WT seq	WT IC50	MUT seq	MUT IC50
1	Zbtb40 NM_198248	G2303C / R768P	KSFHFYCRL	2.9	KSFHFYCPL	3.3
36	Dpagt1 NM_007875	G637T / V213L	ASIIVFNLV	609.4	ASIIVFNLL	118.9
42	Cry1 NM_007771	G1246T / V416L	QFFHCYCPV	781.2	QFFHCYCPL	164.7

Figure 3. Neoantigen Screening from PD-L1-KO Tumors

(A) Circos plot showing the detected mutations in the MC38 tumor. Tumor tissues were sampled at day 15 after tumor inoculation. Mutations of MC38 were identified by whole-exome sequence and RNA sequencing (RNA-Seq). FPKM value and MHC-I affinity values were also plotted.

(B) Venn diagram of identified missense mutations between MC38 WT and PD-L1-KO tumors. Reactive peptide sequences and their IC50 values as calculated by NetMHCpan ver3.0. H2-K^b-restricted peptides for MC38 neoantigen candidates were synthesized and prepared.

Figure 3. *Continued*

(C) Experimental scheme of neoantigen candidate screening. MC38-PD-L1-KO tumor-bearing mice were treated with anti-PD-1 and anti-CTLA-4 on day 7, 10, and 13. Fifteen days after tumor inoculation, CD8 T cells were purified from pooled splenocytes and the tumor draining lymph node (4 mice per experiment) and cocultured with 30 Gy-irradiated splenocytes in the presence or absence of 10 μg/mL neoantigen candidate peptides for 72 h.

(D) Upper, culture supernatants were measured for IFN-γ production by ELISA. Data are pooled from five independent experiments. Lower, character of neoantigen peptides.

induction and PD-L1 expression on tumors, we evaluated the combined ICB treatment (anti-PD-1 Ab plus anti-CTLA-4 Ab) against MC38 or MC38-PD-L1-KO tumor cells *in vivo*. The tumor regression was more effective in ICB-treated MC38-PD-L1-KO tumor-cell-bearing mice than ICB-treated MC38 tumor-bearing mice or non-treated MC38-PD-L1-KO tumor-cell-bearing mice (Figure 2C).

Due to the enhanced antitumor effect in MC38-PD-L1-KO mice, we hypothesized two possibilities: (1) the balance of immune responses was altered in MC38-PD-L1-KO and (2) T cells responded to neoantigens that were more expressed in MC38-PD-L1-KO. As such, we analyzed the immune responses two weeks later in MC38 or MC38-PD-L1-KO mice when no difference in tumor size was observed. As shown in Figure 2D, there was no statistical difference in the frequency of various types of immune cells including T and natural killer (NK) cells. Next, we assessed the CTL function. As shown in Figure 2C, growth of MC38-PD-L1-KO cells in ICB-treated mice progressed slowly and retarded two weeks after subcutaneous tumor inoculation. Therefore, we analyzed the T cell response for the previously identified H2-D^b restricted antigen, mutant (Mut) Adpgk, and H2-K^b restricted antigen, p15E, on day 15. In ICB-treated MC38-PD-L1-KO bearing mice, we detected the apparent MutAdpgk-specific $CD8^+$ T cell infiltration in the tumor (Figure 2E). We also assessed their functions using exhaustion/activation markers and found the differential presence of PD-1^+Tim-3^+ or PD-1^+CD69^+ responsive $CD8^+$ T cells in MC38-KO tumor compared with MC38 WT tumor (Figure S3). Moreover, $CD8^+$ T cells in the spleen and lymph nodes of these mice responded well to p15E and MutAdpgk antigens (Figure S4). Thus, the ICB-treated mice injected with MC38-PD-L1-KO enhanced the apparent antigen-specific T cell response.

Screening of H2-K^b-Restricted Neoantigens by Exome and Transcriptome Analyses

MutAdpgk was previously reported as a type of neoantigen, expressed on H2-D^b of MC38 (Yadav et al., 2014). We speculated that neoepitopes on other MHCs could be identified, and thus a mixture of antigens, composed of different MHC-restricted neoantigens, would be more efficient as vaccines. Therefore, we conducted exome and transcriptome sequences of MC38 and MC38-PD-L1-KO tumor tissues to identify tumor-specific point mutations with amino acid substitutions, including stop gain, frameshift, and missense mutations (Figure 3A). Further, putative neoepitopes were found to be randomly distributed throughout the genome. First, to identify single-nucleotide variants (SNVs), data derived from the exome and RNA sequences obtained from MC38 or MC38-PD-L1-KO were compared with normal mouse blood (Figure S5A). As a result, 7,683 and 6,876 coding variants with almost similar mutation signature were identified by exome sequencing (Figure S5B), and subsequently 826 and 775 by RNA-seq, which overlapped with the exome-based variants, in MC38 and MC38-PD-L1-KO, respectively. Among these, 808 and 755 missense mutations were found in MC38 and MC38-KO, respectively. Common major mutated epitopes in MC38 and MC38-PD-L1-KO were observed to harbor 645 potential epitopes that might be stable or universal (Figure 3B). By contrast, mutated epitopes in MC38 alone or MC38-PD-L1-KO alone were 163 and 110, respectively (Figure 3B). Nevertheless, the rates of mutation detected in both transcriptome and exome analyses were similar: 826/7683 = 0.107 (WT) and 755/6876 = 0.113 (PD-L1-KO). Although some mutations disappeared and other novel mutations possibly appeared in PD-L1-KO tumor probably due to immunoediting or clonal evolution in a broad sense, majority of the missense mutations was shared. Therefore, we hypothesized that common CTL responses against parental tumors may be present in PD-L1-KO tumor-bearing mice, by which augmented CTL responses enable high sensitive screening of tumor-specific response as shown in Figures 2E and S4.

High Immunogenic Neoantigens Identified by Immunome Analyses

SNVs were analyzed for their potential to generate MHC-I-restricted epitopes of the murine H2-K^b alleles using the NetMHCpan algorithm. We selected neoantigen candidates presented on H2-K^b (predicted IC50 < 200, rank <1) from common missense mutations in both WT and PD-L1-KO tumors using the NetMHCpan (ver 3.0) algorithm (Nielsen and Andreatta, 2016). Overall, 49 peptides derived from abundant transcripts were more likely to be presented on MHC-I of MC38 cells. Next, we evaluated the

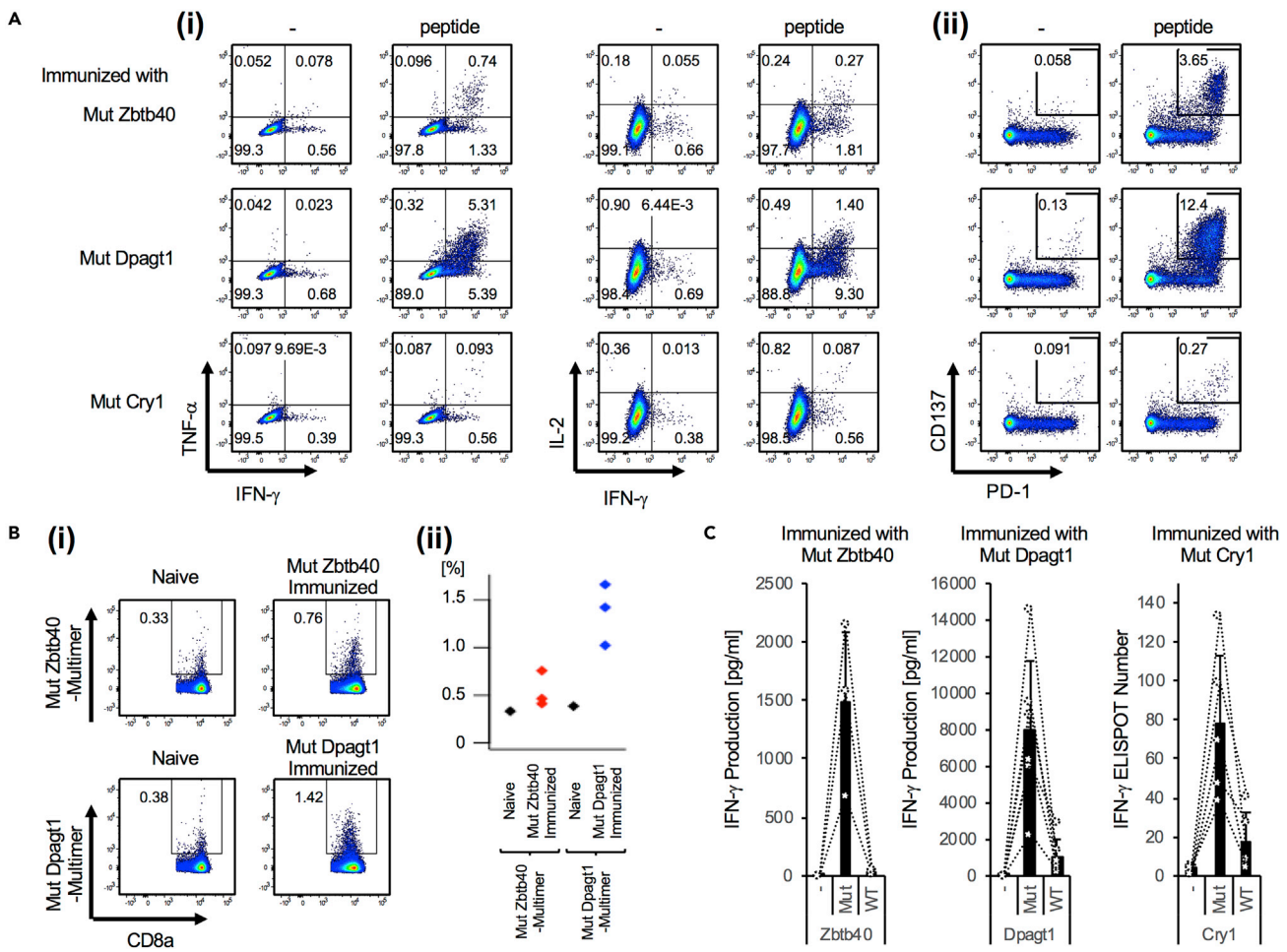

Figure 4. Bioactive Neoantigen Epitopes

Analysis of neoantigen-specific T cells in vaccinated mice. C57BL/6J mice were administered intravenously (i.v.) with neoantigen peptide (Zbtb40, Dpagt1, and Cry1) together with poly(I:C) and anti-CD40 Ab.

(A) One week later, neoantigen-specific T cell activation in these mice was assessed by intracellular staining for IFN-γ and TNF-α production (i) and upregulation of PD-1 and CD137 (ii) after culturing with or without each peptide for 6 h (i) or 24 h (ii).

(B) As shown in (A), neoantigen-specific T cell proliferating responses in these mice were assessed by multimer-APC, CD8a-FITC, and TCR-β-PE. Representative flow cytometry analysis (i) and each value was plotted (ii).

(C) Neoantigen-specific T cell response was quantified. Whole splenocytes (ELISA) or isolated $CD8^+$ T cells (ELISPOT) from mice given each neoantigen were cultured with each neoantigen peptide or non-mutated relevant peptide for 24 h and assessed for IFN-γ production. Data are pooled from two independent experiments, and the values represent mean ± SD. Circles and dot lines link respective mice.

immunogenicity of mutated tumor antigens *in vivo*. By utilizing PD-L1-KO tumors, one week after tumor inoculation, the tumor-bearing mice were treated three times with ICB combination therapy. $CD8^+$ T cells from the spleen and lymph nodes were harvested and stimulated with or without 49 types of epitope candidate peptides for 72 h. IFN-γ production as an indicator of $CD8^+$ T cell responses was measured (Figure 3C). With this screening, significant IFN-γ production was shown by culturing in the presence of #1 (Zbtb40 R768P), #36 (Dpagt1 V213L), and #42 (Cry1 V416L) (Figure 3D).

To examine whether these three predicted peptides could elicit $CD8^+$ T cell responses, we administered each peptide to WT mice together with anti-CD40 Ab plus poly(I:C). We demonstrated that $CD8^+$ T cells specific for MutZbtb40, MutDpagt1, and MutCry1 antigens, respectively, produced IFN-γ, TNF-α, and IL-2 (Figure 4Ai) and expressed $CD137^+PD1^+$ $CD8^+$ T cells in an antigen-specific manner (Figure 4Aii). We also demonstrated that antigen-specific $CD8^+$ T cells responded to MutZbtb40 or MutDpagt1 neoantigen by multimer staining (Figure 4Bi, ii) and ELISA or ELISPOT assay (Figure 4C), but they did not respond

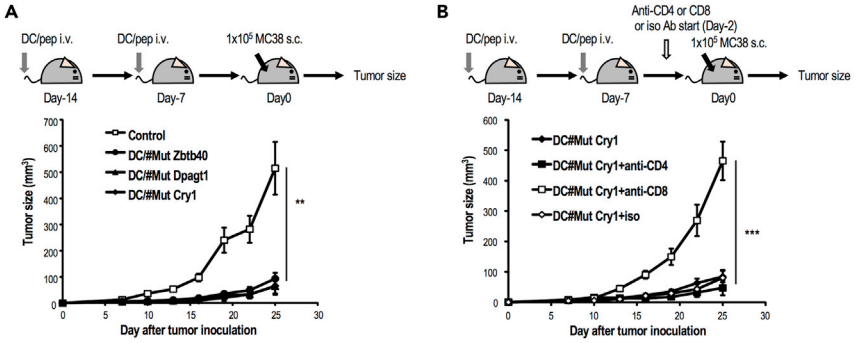

Figure 5. Demonstration of Antitumor Response by Neoantigen-Pulsed DCs Therapy

(A) Immunogenicity of neoantigen *in vivo* using prophylactic tumor model. Bone-marrow-derived dendritic cells (BM-DCs) were generated as previously reported. Each peptide-pulsed BM-DC (1×10^6/mouse) was intravenously injected twice to WT mice at day 14 and 7. Immunized mice were challenged with 1×10^5 MC38 tumor cells s.c. Tumor growth was monitored at indicated time points (mean ± SEM, n = 8/group).

(B) MutCry1-peptide-pulsed DCs (1×10^6/mouse) were administered to WT mice. Vaccinated mice were challenged with 1×10^5 MC38 tumor cells. In some experiments, mice were treated with anti-CD4 Ab or anti-CD8 Ab 2 days before tumor injection and repeatedly during tumor monitoring. Tumor growth was monitored at indicated time points (mean ± SEM, n = 7/group). Data are pooled from two independent experiments and analyzed by one-way ANOVA followed by Turkey's multiple comparison test. $^{**}p < 0.001$, $^{***}p < 0.001$.

to the non-mutated original antigen. Thus, through a computational approach and analysis of their immunogenic antigen-specific properties and biological analyses, these three predicted neoantigen peptides were determined to be immunogenic in the context of MC38 tumors.

Vaccination with Neoantigen-Peptide-pulsed DCs Demonstrates Tumor Protection

Different from self-antigen-derived, conventional tumor antigens, neoantigens are specific and powerful. Because DCs are known as the most powerful antigen-presenting cells (APCs) for priming T cells in murine and humans, *ex vivo*-expanded DCs are of interest. We initially assessed the antitumor effect using neoantigen-pulsed DC therapy in prophylactic models. To determine if $CD8^+$ T cells induced against neoepitopes could provide protective anti-tumor immunity, C57BL/6J mice were administered with the mutated peptide (Zbtb40, Dpagt1, and Cry1)-pulsed DCs and then subsequently challenged with 1×10^5 MC38 tumor cells (Figure 5A). Tumor growth was inhibited in most animals in each neoantigen-pulsed DC vaccine group (Figure 5A). This protection in mice immunized with MutCry1-peptide-pulsed DCs was absent in anti-CD8 Ab-treated mice, but not anti-CD4 Ab-treated mice, strongly supporting that $CD8^+$ T cell responses specific to mutated peptides conferred protection (Figure 5B).

Next, we evaluated the therapeutic potential of each single peptide by comparing mixed neoantigens in the antitumor-specific T cell response. For this study, the treatment with a single neoantigen-pulsed DCs was followed by peptide with anti-CD40 Ab and Poly(I:C), which induces robust T cell responses (Nimanong et al., 2017). We monitored the number of tumor-bearing mice that did not exceed 400 mm^3 of tumor size until day 25 and found that 40% of mice (i.e., 5/13, 6/13, and 7/13) treated with each of the neoantigen-pulsed DCs had smaller tumors on day 25 (Figure 6A). In addition, vaccinated mice with mixed peptide (Z + D + C)-pulsed DCs showed a greater antitumor effect, similar to MutAdpgk (Figure 6A). Thus, vaccination with neoantigens showed remarkable and sustainable inhibition of tumor growth. In addition, we found that the frequency of the three mixed-peptide-reactive $CD8^+$ T cells that were capable of producing IFN-γ (left), IFN-γ/TNF-α (middle), or IL-2/IFN-γ/TNF-α (right) were increased at the tumor site (Figures 6B, 6C, S6A, and S6B). On the other hand, we detected the slight levels of MutAdpgk-specific IFN-γ-/TNF-α-producing T cells (Figures 6B and 6C). Thus, we observed an enhancement of the multifunctional $CD8^+$ T cell response to three peptides in mice vaccinated with three neoantigen-peptide DCs. In addition, the $CD8^+$ T cell response against MutAdpgk was generated in mice vaccinated with MutAdpgk-peptide DCs to a similar extent as with three peptide-pulsed DCs. These suggest that neoantigen-responding T cells by vaccination with peptide-pulsed DCs are multifunctional in an antigen-specific manner and imply that even when with neoantigens of low antigenicity, the mixed-peptide-pulsed DC therapy would be useful.

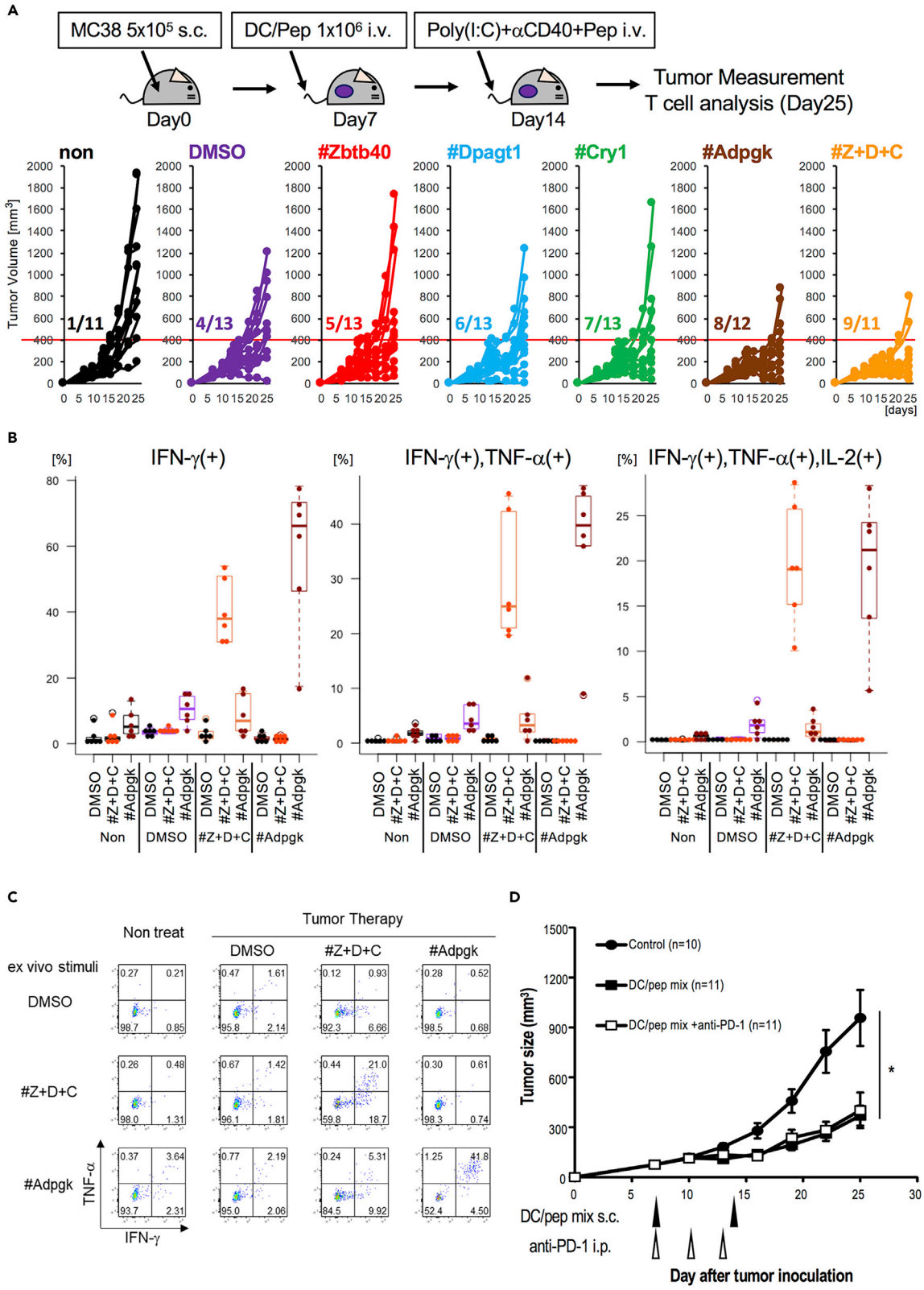
A
MC38 5x10⁵ s.c.
DC/Pep 1x10⁶ i.v.
Poly(I:C)+αCD40+Pep i.v.
Day0
Day7
Day14
Tumor Measurement
T cell analysis (Day25)
non
DMSO
#Zbtb40
#Dpagt1
#Cry1
#Adpgk
#Z+D+C
Tumor Volume [mm³]
1/11
4/13
5/13
6/13
7/13
8/12
9/11
[days]
B
IFN-γ(+)
IFN-γ(+),TNF-α(+)
IFN-γ(+),TNF-α(+),IL-2(+)
[%]
DMSO
#Z+D+C
#Adpgk
Non
DMSO
#Z+D+C
#Adpgk
C
Non treat
Tumor Therapy
DMSO
#Z+D+C
#Adpgk
ex vivo stimuli
DMSO
#Z+D+C
#Adpgk
TNF-α
IFN-γ
D
Control (n=10)
DC/pep mix (n=11)
DC/pep mix +anti-PD-1 (n=11)
Tumor size (mm³)
*
DC/pep mix s.c.
anti-PD-1 i.p.
Day after tumor inoculation

Figure 6. Comparison of Therapeutic Effect by Single Epitope or Multiple Epitopes of Neoantigen

(A) Tumor therapeutic model. C57BL/6J mice were s.c. injected with MC38 tumor cells and treated with neoantigen single-peptide- or multipeptide-pulsed DCs at a week later and again with the relevant peptide together with poly(I:C) and anti-CD40 Ab. Tumor growth was monitored at indicated time points. Tumor growth curve in each group of mice was plotted. As shown by the red line, tumor volume <400 mm^3 at day 25 was consider as a partial response. Data are pooled from five independent experiments (n = 11–13).

(B and C) Analysis of TIL in mice treated with multipeptides of neoantigens. TILs were stimulated by peptides in the presence of anti-CD28 and brefeldin. (B) The percentages of IFN-γ single-producing T cells (left), IFN-γ^+TNF-α^+-producing T cells (middle), and IFN-γ^+TNF-α^+IL-2^+-producing T cells (right) were plotted. Data are pooled from three independent experiments (n = 6). (C) Representative flow cytometry analysis of $CD8^+$ TILs shows IFN-γ and TNF-α.

(D) Therapeutic effect by neoantigen-pulsed DCs. MC38 cells were administered s.c. One week later, these mice were treated with neoantigen-pulsed DCs twice at 1-week intervals. Anti-PD-1 Ab was injected intraperitoneally (i.p.) at day 7, 10, and 13 (n = 10 and 11/group). Data are pooled from four independent experiments, and the values represent mean ± SEM. Data were analyzed by one-way ANOVA followed by Turkey's multiple comparison test. *$p < 0.05$.

Apparently, these are immunodominant neoepitopes. Further, these results show that $CD8^+$ T cell responses are generated by vaccination with peptide-pulsed DCs against neoepitopes in MC38 tumors. To evaluate the immunotherapy using neoantigen-pulsed DC, we examined the antitumor therapeutic effect using mixed neoantigen peptides, including one Adpgk H2-D^b- and three H2-K^b-restricted-peptide-pulsed (Z + D + C) DCs in MC38 tumor-bearing mice. As shown in Figure 6D, there was an extensive therapeutic effect. When we examined whether neoantigen-pulsed DCs and ICB therapy could synergistically inhibit tumor growth, we found that antitumor immunity induced by neoantigen-pulsed DCs was at a sufficient level, such that an additional effect by the anti-PD-1 Ab could not augment the response further (Figure 6D). In its therapeutic effect, single-agent anti-PD-1 Ab caused around 43% tumor reduction at day 25 (Figure S2D). In contrast, DC/Pep mix yielded 58% tumor reduction compared with WT tumors. Therefore, instead of ICB treatment, vaccination with DCs pulsed with neoepitope peptides generated sufficient T cell immunity to inhibit established tumors.

Neoantigen-Reactive TCR Recognizes Parental MC38 Tumor Cells

Because we showed that mutation-specific peptide selected by biological assay induced tumor-reactive T cells, we next attempted to identify the T cell receptor (TCR) repertoire of antigen-specific T cell clones that could be elicited by each neoantigen. A detailed analysis of the phenotypes of these T cell clonotypes and the biophysical properties of the TCR may shed light on the extent, depth, and requirements for efficient T cell responses against tumors. We isolated neoantigen-reactive T cells by FACS sorting of the $CD8^+$ multimer$^+$ CTL reactive for MutDpagt1 or $CD8^+$PD-$1^+$$CD137^+$ T cells reactive for MutCry1 (Figure S7A, left). We cloned each TCRα and TCRβ sequence into a retroviral vector (pMXs), followed by transfection into the TG40 cell line (Figure S7A, right). The top five sequences of repertoire analysis were selected, and orange- and green-colored ones were subcloned into the expression vector (Figure S7B). To verify that the sequences of the α and β chain were indeed candidates for neoantigen-reactive TCRα and β, we cocultured the TCR-gene-modified TG40 cells with peptide-pulsed EL4. As shown in Figures S7C and S7D, we found one combination of TCRα and TCRβ in MutDpagt1, whereas two combinations of TCRα and TCRβ were found in MutCry1 for CD69 upregulation, suggesting that they are unique and clonal TCRs. Because TCRs shared the conserved CDR3 sequences for recognizing the same MHC-I epitopes, clustering TCRs based on sequence motif enables epitope-specific recognition and diversity. We parsed randomly extracted repertoire sequences by TCRdist (Dash et al., 2017) for TCRB clustering. We observed the homology-based hierarchy and found that neoantigen reactive TCRs occurred in groups (red triangle) and these cluster-relevant newly established sequences in CDR3 during VDJ recombination (framed red; Figure 7A). These new motifs were shown to frequently interact with MHC-I epitopes by crystal structure analysis. Therefore, to confirm that these neoantigens could induce specific responses, we synthesized mutated di-amino acids sequences, AlaAla, into the CDR3 region. As expected, AlaAla mutation-harboring TCRs drastically lost their reactivity to neoantigens. Moreover, we performed mutant and WT peptide titration assays (Figure S8) and confirmed strong specificity of the neoantigen mutation for TCR8 and TCR10, which was weak for TCR36 (Figures 7B, 7C, and S8). We observed a slight, but apparent, specificity of TCR36 (for Dpagt1) and TCR8 and 10 (for Cry1) by a mutant and WT peptide titration. These suggested that several clonotypes could be generated from the same mutated specific peptide (Cry1 peptide).

Finally, we examined whether antigen-specific TCRα and β chain-bearing T cells could respond to each peptide antigen and parental MC38 tumor cells. In primary T cells transduced with TCRα and TCRβ gene, even without neoantigens peptides, TCRs reacted with MC38 and produced IFN-γ (Figure 7D). Regarding the tumor response, not only TCR36 but also TCR8 and TCR10 could respond to MC38. Thus, tumor neoantigen-specific T cell clones exhibited antigen-specific responses against MC38.

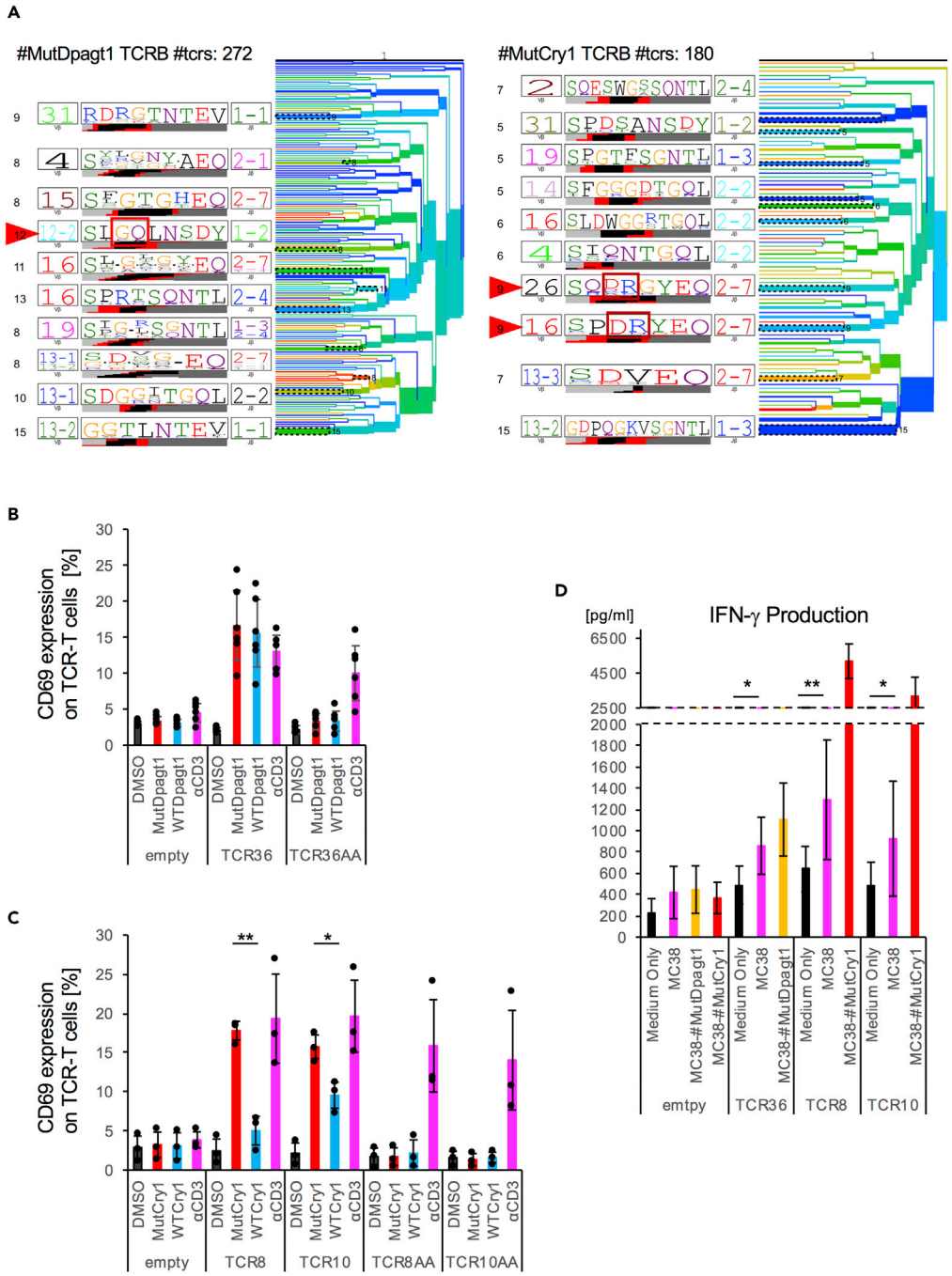

Figure 7. Primary T Cell Expressing Neoantigen-Specific TCR Recognizes Tumor

(A) TCRdist analysis of TCRB repertoire sequences showing the tree diagram of TCRB CDR3 homology. Clonality was not reflected. Red arrows indicate neoantigen peptide reactive CDR3 sequence. As a negative control, rearranged CDR3-derived di-amino acids (red rectangle) were mutated into AlaAla.

(B and C) TCRαβ derived from CTL responding to Dpagt1pep included TCR36, and TCRαβ derived from CTL responding to Cry1pep is termed as TCR8 and TCR10. Reactive TCRα and β chains were selected, and they were tandemly linked with Furin-SGSG-P2A sequence and cloned into pMXs-IRES-GFP. Selected combination of TCRα and TCRβ were transfected to TG40 CD8A/B (TCR36, B; TCR8, TCR10, C). These TG40 cells were cocultured with each peptide-pulsed EL4 for 24 h. The percentage of CD69 upregulation by TCR36 or TCR8 and TCR10 and their AA mutation transduction in GFP^+ cells for MutDapgt1 peptide or MutCry1 peptide is shown. Data were pooled from six or three independent experiments, and the values represent mean ± SD. Each black circle shows independent values.

Figure 7. *Continued*

(D) TCR36-transduced or TCR8- and TCR10-transduced GFP$^+$CD8$^+$ T cells were cocultured with MC38 in the presence or absence of neoantigens peptide for 48 h. Subsequently, supernatants were measured for IFN-γ by ELISA. Data were pooled from seven to ten independent experiments, and the values represent mean ± SD. Data were analyzed by unpaired Student's t test, *p < 0.05, **p < 0.01.

DISCUSSION

The TME is associated with response to ICB therapy. Particularly, PD-L1 expression, the frequency of CD8$^+$ T cell infiltration, and the mutation burden in tumors correlate well with the likelihood of response during or after ICB therapy. However, the biological relevance of each of these factors has to be clarified for effective ICB usages. In this study, we showed that the difference between resistance and sensitivity of ICB tumors depended on the responsiveness of T cells to neoantigens as a key T cell response in tumor sites. Particularly, we demonstrated the relationship between PD-L1 expression on tumors and the sensitivity to ICB therapy by comparing ICB-treated MC38-PD-L1-KO (non-innate resistant type) and parental MC38 (innate resistant type). In fact, when tumors express PD-L1, even if they have the potential to generate an antitumor T cell response by ICB therapy, these T cells are weak, resulting in faster tumor growth. In contrast, when tumors lack PD-L1, the antitumor T cell immunity against neoantigens can be significantly elicited by ICB, resulting in slowed growth of the tumor.

A tumor-intrinsic role of PD-L1 is to promote cancer initiation toward CSC metastasis, progression, and resistance to therapy (Dong et al., 2018; Fabrizio et al., 2018). In *in vitro* studies, disruption of intrinsic PD-L1 by CRISPR/Cas9 technique led to suppression of progressive cancer cells, inhibition of spheroid formation of osteosarcoma, and increased anticancer drug sensitivities to doxorubicin and paclitaxel (Liao et al., 2017). PD-L1 transactivation pathway is likely abnormal in many cancers. In intrinsic mechanisms underlying aberrant PD-L1 activation, genomic alterations (i.e., copy number amplification of CD274 residues (Cancer Genome Atlas Research Network, 2014; Straub et al., 2016; George et al., 2017) and 3′-UTR disruption (Schoenberg and Maquat, 2012; Kataoka et al., 2016)), constitutive oncogenic signaling activation (via PI3K/AKT or RAS/MAPK (Crane et al., 2009; Coelho et al., 2017)), and epigenetic changes (e.g., expression of microRNA 197 during PD-L1 inhibition in lung cancer and aberrant DNA methylation (Fujita et al., 2015; Dong et al., 2016)) have been described. Whereas, as extrinsic factors, IFN-γ (Garcia-Diaz et al., 2017) and other inflammatory cytokines (e.g., IL-17 and TNF-α) (Wang et al., 2017) and HIF-1α (Noman et al., 2014) can activate PD-L1. Hence, what determines the low PD-L1 expression in highly immunogenic TME, which presumably drives best clinical benefits from ICB therapy, needs to be investigated in the future studies.

Effective antitumor vaccines using neoantigens are often the most immunogenic. In the current study, we identified novel three neoantigens on MC38 in an H2-K^b-restricted manner and showed the potential utility of a neoantigen-mixed peptides-pulsed DC vaccine beyond the PD-L1-restricted mechanism. DCs are essential in immunity owing to their role in activating T cells, thereby promoting antitumor responses. Compared with the clinical success of *ex vivo* DC therapy based on conventional tumor antigens, neoantigen-pulsed DCs have been anticipated for showing potent efficacy (Carreno et al., 2015; Chen et al., 2019). In fact, in this study, we exhibited the efficacy of four types of neoantigen-responding T cells infiltrating in the tumor in mice treated with four neoantigen-peptide-pulsed DCs. Moreover, we demonstrated that neoantigen-specific T cells in TME by DC vaccination possess multifunctionality and an antitumor effect similar to ICB therapy. It is known that anti-CTLA-4 Ab acts through APCs, particularly on DCs, leading to CTL generation, whereas anti-PD-1 Ab therapy can reactivate an impaired CTL. Effectiveness of ICB therapy must depend on DC function. Further, neoantigen-pulsed DC vaccines improved T cell responses in tumors, at levels similar to those by ICB therapy. These support ICB sensitivity dependences on CD8$^+$ T cell responses specific to "multiple" neoantigens, conferring protection against tumors. Combination therapy using ICB may have clinical benefits, but a major limitation remains its characteristic antigen loss. Particularly, it is known that ICB efficacy can be impaired by deleting neoantigens on tumors, which results in tumor progression (Tran et al., 2016). In this study, using different MHC-restricted tumor-associated neoantigens simultaneously with mature DCs, we suggested that starting therapy using multiple neoantigen-peptide-pulsed DCs at early phase generates clinically relevant neoantigen-specific T cells before possible deletion and immune evasion.

Taken together, our findings provide tumor immunological evidence that the level of T cell responses to neoantigens and PD-L1 expression on tumor determine the positive and negative cancer immunity cycle, and therefore, may shape immunoediting during tumor occurrence, which must be optimally targeted for

clinical responses. In addition, our results suggested that PD-L1-KO tumor cells may be useful in isolating neoantigen-specific T cells and that identified neoantigen vaccination could block immune escape, highlighting the recently refocused development in DC cancer vaccines against immune checkpoint ligand-expressing tumors (Figure S9).

Limitation of the Study

In this study, we clarified the innate resistance roles of PD-L1-expressing tumor, which dampens tumor-specific CTLs responses including neoantigens. The fact that PD-L1-deficient tumors treated with anti-PD-1Ab plus anti-CTLA-4 Ab facilitated the neoantigens screen with higher sensitivity may indicate the usefulness of applicable DC-based vaccines. This approach may extend to the clinical application. However, in the current study, the identification of neoantigens were derived from *in vivo* studies in murine. There are still several problems to identify the neoantigens in human. We need to make new *in vitro* protocol or new method to use humanized mice for identification of neoantigens.

Resource Availability

Lead Contact

Further information is available from the Lead Contact, Shin-ichiro Fujii (shin-ichiro.fujii@riken.jp).

Materials Availability

Requests for resources and reagents should be directed to and will be fulfilled by the Lead Contact.

Data and Code Availability

The accession number for the Exome and RNA sequence datasets reported in this paper is DNA Data Bank of Japan (DDBJ) Sequence Read Archive (DRA):DRA010264. The request for additional data or codes not infringing on ethics restrictions is available to Lead Contact.

METHODS

All methods can be found in the accompanying Transparent Methods supplemental file.

SUPPLEMENTAL INFORMATION

Supplemental Information can be found online at https://doi.org/10.1016/j.isci.2020.101238.

ACKNOWLEDGMENTS

This work was supported by JSPS KAKENHI Grant Number JP19K07653.

AUTHOR CONTRIBUTIONS

S.F., M.O., and K.S. conceived and designed the experiments. Y.M., T.W., and O.O performed bioinformatics analysis for potential neoepitopes. T.W. conducted and analyzed RNA sequencing data, and M.O. detected the TCR repertoire. J.S. established the cassette of TCRA and TCRB genes, and M.O. generated the final TCRA and TCRB. M.O. mainly, K.S., S.U., and T.I. performed the biological studies, and S.F., M.O., K.S., and T.I conducted data analysis. S.F. supervised the overall project. S.F. and M.O. wrote the manuscript with input from all the other authors.

DECLARATION OF INTERESTS

The authors have no financial conflicts of interest related to this manuscript.

Received: January 7, 2020
Revised: May 4, 2020
Accepted: June 2, 2020
Published: June 26, 2020

REFERENCES

Ahmadzadeh, M., Johnson, L.A., Heemskerk, B., Wunderlich, J.R., Dudley, M.E., White, D.E., and Rosenberg, S.A. (2009). Tumor antigen-specific CD8 T cells infiltrating the tumor express high levels of PD-1 and are functionally impaired. Blood *114*, 1537–1544.

Bezu, L., Kepp, O., Cerrato, G., Pol, J., Fucikova, J., Spisek, R., Zitvogel, L., Kroemer, G., and Galluzzi, L. (2018). Trial watch: peptide-based vaccines in anticancer therapy. Oncoimmunology *7*, e1511506.

Bol, K.F., Figdor, C.G., Aarntzen, E.H., Welzen, M.E., van Rossum, M.M., Blokx, W.A., van de Rakt, M.W., Scharenborg, N.M., de Boer, A.J., Pots, J.M., et al. (2015). Intranodal vaccination with mRNA-optimized dendritic cells in metastatic melanoma patients. Oncoimmunology *4*, e1019197.

Bottcher, J.P., and Reis, E.S.C. (2018). The role of type 1 conventional dendritic cells in cancer immunity. Trends Cancer *4*, 784–792.

Brahmer, J., Reckamp, K.L., Baas, P., Crino, L., Eberhardt, W.E., Poddubskaya, E., Antonia, S., Pluzanski, A., Vokes, E.E., Holgado, E., et al. (2015). Nivolumab versus docetaxel in advanced squamous-cell non-small-cell lung cancer. N. Engl. J. Med. *373*, 123–135.

Cancer Genome Atlas Research Network (2014). Comprehensive molecular characterization of gastric adenocarcinoma. Nature *513*, 202–209.

Carreno, B.M., Magrini, V., Becker-Hapak, M., Kaabinejadian, S., Hundal, J., Petti, A.A., Ly, A., Lie, W.R., Hildebrand, W.H., Mardis, E.R., et al. (2015). Cancer immunotherapy. A dendritic cell vaccine increases the breadth and diversity of melanoma neoantigen-specific T cells. Science *348*, 803–808.

Castle, J.C., Kreiter, S., Diekmann, J., Lower, M., van de Roemer, N., de Graaf, J., Selmi, A., Diken, M., Boegel, S., Paret, C., et al. (2012). Exploiting the mutanome for tumor vaccination. Cancer Res. *72*, 1081–1091.

Chen, F., Zou, Z., Du, J., Su, S., Shao, J., Meng, F., Yang, J., Xu, Q., Ding, N., Yang, Y., et al. (2019). Neoantigen identification strategies enable personalized immunotherapy in refractory solid tumors. J. Clin. Invest. *129*, 2056–2070.

Coelho, M.A., de Carne Trecesson, S., Rana, S., Zecchin, D., Moore, C., Molina-Arcas, M., East, P., Spencer-Dene, B., Nye, E., Barnouin, K., et al. (2017). Oncogenic RAS signaling promotes tumor immunoresistance by stabilizing PD-L1 mRNA. Immunity *47*, 1083–1099.e6.

Crane, C.A., Panner, A., Murray, J.C., Wilson, S.P., Xu, H., Chen, L., Simko, J.P., Waldman, F.M., Pieper, R.O., and Parsa, A.T. (2009). PI(3) kinase is associated with a mechanism of immunoresistance in breast and prostate cancer. Oncogene *28*, 306–312.

Dash, P., Fiore-Gartland, A.J., Hertz, T., Wang, G.C., Sharma, S., Souquette, A., Crawford, J.C., Clemens, E.B., Nguyen, T.H.O., Kedzierska, K., et al. (2017). Quantifiable predictive features define epitope-specific T cell receptor repertoires. Nature *547*, 89–93.

Dong, P., Xiong, Y., Watari, H., Hanley, S.J., Konno, Y., Ihira, K., Suzuki, F., Yamada, T., Kudo, M., Yue, J., et al. (2016). Suppression of iASPP-dependent aggressiveness in cervical cancer through reversal of methylation silencing of microRNA-124. Sci. Rep. *6*, 35480.

Dong, P., Xiong, Y., Yue, J., Hanley, S.J.B., and Watari, H. (2018). Tumor-intrinsic PD-L1 signaling in cancer initiation, development and treatment: beyond immune evasion. Front. Oncol. *8*, 386.

Eggermont, A.M.M., Blank, C.U., Mandala, M., Long, G.V., Atkinson, V., Dalle, S., Haydon, A., Lichinitser, M., Khattak, A., Carlino, M.S., et al. (2018). Adjuvant pembrolizumab versus placebo in resected stage III melanoma. N. Engl. J. Med. *378*, 1789–1801.

Fabrizio, F.P., Trombetta, D., Rossi, A., Sparaneo, A., Castellana, S., and Muscarella, L.A. (2018). Gene code CD274/PD-L1: from molecular basis toward cancer immunotherapy. Ther. Adv. Med. Oncol. *10*, 1758835918815598.

Ferris, R.L., Blumenschein, G., Jr., Fayette, J., Guigay, J., Colevas, A.D., Licitra, L., Harrington, K., Kasper, S., Vokes, E.E., Even, C., et al. (2016). Nivolumab for recurrent squamous-cell carcinoma of the head and neck. N. Engl. J. Med. *375*, 1856–1867.

Fujii, S., Fujimoto, K., Shimizu, K., Ezaki, T., Kawano, F., Takatsuki, K., Kawakita, M., and Matsuno, K. (1999). Presentation of tumor antigens by phagocytic dendritic cell clusters generated from human CD34+ hematopoietic progenitor cells: induction of autologous cytotoxic T lymphocytes against leukemic cells in acute myelogenous leukemia patients. Cancer Res. *59*, 2150–2158.

Fujii, S., Liu, K., Smith, C., Bonito, A.J., and Steinman, R.M. (2004). The linkage of innate to adaptive immunity via maturing dendritic cells in vivo requires CD40 ligation in addition to antigen presentation and CD80/86 costimulation. J. Exp. Med. *199*, 1607–1618.

Fujii, S., Shimizu, K., Hemmi, H., and Steinman, R.M. (2007). Innate Valpha14(+) natural killer T cells mature dendritic cells, leading to strong adaptive immunity. Immunol. Rev. *220*, 183–198.

Fujii, S.I., and Shimizu, K. (2019). Immune networks and therapeutic targeting of iNKT cells in cancer. Trends Immunol. *40*, 984–997.

Fujita, Y., Yagishita, S., Hagiwara, K., Yoshioka, Y., Kosaka, N., Takeshita, F., Fujiwara, T., Tsuta, K., Nokihara, H., Tamura, T., et al. (2015). The clinical relevance of the miR-197/CKS1B/STAT3-mediated PD-L1 network in chemoresistant non-small-cell lung cancer. Mol. Ther. *23*, 717–727.

Garcia-Diaz, A., Shin, D.S., Moreno, B.H., Saco, J., Escuin-Ordinas, H., Rodriguez, G.A., Zaretsky, J.M., Sun, L., Hugo, W., Wang, X., et al. (2017). Interferon receptor signaling pathways regulating PD-L1 and PD-L2 expression. Cell Rep. *19*, 1189–1201.

George, J., Saito, M., Tsuta, K., Iwakawa, R., Shiraishi, K., Scheel, A.H., Uchida, S., Watanabe, S.I., Nishikawa, R., Noguchi, M., et al. (2017). Genomic amplification of CD274 (PD-L1) in small-cell lung cancer. Clin. Cancer Res. *23*, 1220–1226.

Gryfe, R., Kim, H., Hsieh, E.T., Aronson, M.D., Holowaty, E.J., Bull, S.B., Redston, M., and Gallinger, S. (2000). Tumor microsatellite instability and clinical outcome in young patients with colorectal cancer. N. Engl. J. Med. *342*, 69–77.

Herbst, R.S., Soria, J.C., Kowanetz, M., Fine, G.D., Hamid, O., Gordon, M.S., Sosman, J.A., McDermott, D.F., Powderly, J.D., Gettinger, S.N., et al. (2014). Predictive correlates of response to the anti-PD-L1 antibody MPDL3280A in cancer patients. Nature *515*, 563–567.

Hodi, F.S., Chesney, J., Pavlick, A.C., Robert, C., Grossmann, K.F., McDermott, D.F., Linette, G.P., Meyer, N., Giguere, J.K., Agarwala, S.S., et al. (2016). Combined nivolumab and ipilimumab versus ipilimumab alone in patients with advanced melanoma: 2-year overall survival outcomes in a multicentre, randomised, controlled, phase 2 trial. Lancet Oncol. *17*, 1558–1568.

Hugo, W., Zaretsky, J.M., Sun, L., Song, C., Moreno, B.H., Hu-Lieskovan, S., Berent-Maoz, B., Pang, J., Chmielowski, B., Cherry, G., et al. (2016). Genomic and transcriptomic features of response to anti-PD-1 therapy in metastatic melanoma. Cell *165*, 35–44.

Juneja, V.R., McGuire, K.A., Manguso, R.T., LaFleur, M.W., Collins, N., Haining, W.N., Freeman, G.J., and Sharpe, A.H. (2017). PD-L1 on tumor cells is sufficient for immune evasion in immunogenic tumors and inhibits CD8 T cell cytotoxicity. J. Exp. Med. *214*, 895–904.

Karasaki, T., Nagayama, K., Kuwano, H., Nitadori, J.I., Sato, M., Anraku, M., Hosoi, A., Matsushita, H., Takazawa, M., Ohara, O., et al. (2017). Prediction and prioritization of neoantigens: integration of RNA sequencing data with whole-exome sequencing. Cancer Sci. *108*, 170–177.

Kataoka, K., Shiraishi, Y., Takeda, Y., Sakata, S., Matsumoto, M., Nagano, S., Maeda, T., Nagata, Y., Kitanaka, A., Mizuno, S., et al. (2016). Aberrant PD-L1 expression through 3'-UTR disruption in multiple cancers. Nature *534*, 402–406.

Kleffel, S., Posch, C., Barthel, S.R., Mueller, H., Schlapbach, C., Guenova, E., Elco, C.P., Lee, N., Juneja, V.R., Zhan, Q., et al. (2015). Melanoma cell-intrinsic PD-1 receptor functions promote tumor growth. Cell *162*, 1242–1256.

Kowanetz, M., Zou, W., Gettinger, S.N., Koeppen, H., Kockx, M., Schmid, P., Kadel, E.E., 3rd, Wistuba, I., Chaft, J., Rizvi, N.A., et al. (2018). Differential regulation of PD-L1 expression by immune and tumor cells in NSCLC and the response to treatment with atezolizumab (anti-PD-L1). Proc. Natl. Acad. Sci. U S A *115*, E10119–E10126.

Le, D.T., Uram, J.N., Wang, H., Bartlett, B.R., Kemberling, H., Eyring, A.D., Skora, A.D., Luber, B.S., Azad, N.S., Laheru, D., et al. (2015). PD-1 blockade in tumors with mismatch-repair deficiency. N. Engl. J. Med. *372*, 2509–2520.

Liao, Y., Chen, L., Feng, Y., Shen, J., Gao, Y., Cote, G., Choy, E., Harmon, D., Mankin, H., Hornicek, F., et al. (2017). Targeting programmed cell death ligand 1 by CRISPR/Cas9 in osteosarcoma cells. Oncotarget *8*, 30276–30287.

Lin, H., Wei, S., Hurt, E.M., Green, M.D., Zhao, L., Vatan, L., Szeliga, W., Herbst, R., Harms, P.W., Fecher, L.A., et al. (2018). Host expression of PD-L1 determines efficacy of PD-L1 pathway blockade-mediated tumor regression. J. Clin. Invest. *128*, 805–815.

McGranahan, N., Furness, A.J., Rosenthal, R., Ramskov, S., Lyngaa, R., Saini, S.K., Jamal-Hanjani, M., Wilson, G.A., Birkbak, N.J., Hiley, C.T., et al. (2016). Clonal neoantigens elicit T cell immunoreactivity and sensitivity to immune checkpoint blockade. Science *351*, 1463–1469.

Motzer, R.J., Tannir, N.M., McDermott, D.F., Aren Frontera, O., Melichar, B., Choueiri, T.K., Plimack, E.R., Barthelemy, P., Porta, C., George, S., et al. (2018). Nivolumab plus ipilimumab versus sunitinib in advanced renal-cell carcinoma. N. Engl. J. Med. *378*, 1277–1290.

Nielsen, M., and Andreatta, M. (2016). NetMHCpan-3.0; improved prediction of binding to MHC class I molecules integrating information from multiple receptor and peptide length datasets. Genome Med. *8*, 33.

Nimanong, S., Ostroumov, D., Wingerath, J., Knocke, S., Woller, N., Gurlevik, E., Falk, C.S., Manns, M.P., Kuhnel, F., and Wirth, T.C. (2017). CD40 signaling drives potent cellular immune responses in heterologous cancer vaccinations. Cancer Res. *77*, 1918–1926.

Noman, M.Z., Desantis, G., Janji, B., Hasmim, M., Karray, S., Dessen, P., Bronte, V., and Chouaib, S. (2014). PD-L1 is a novel direct target of HIF-1alpha, and its blockade under hypoxia enhanced MDSC-mediated T cell activation. J. Exp. Med. *211*, 781–790.

Riaz, N., Morris, L., Havel, J.J., Makarov, V., Desrichard, A., and Chan, T.A. (2016). The role of neoantigens in response to immune checkpoint blockade. Int. Immunol. *28*, 411–419.

Rittmeyer, A., Barlesi, F., Waterkamp, D., Park, K., Ciardiello, F., von Pawel, J., Gadgeel, S.M., Hida, T., Kowalski, D.M., Dols, M.C., et al. (2017). Atezolizumab versus docetaxel in patients with previously treated non-small-cell lung cancer (OAK): a phase 3, open-label, multicentre randomised controlled trial. Lancet *389*, 255–265.

Rizvi, N.A., Hellmann, M.D., Snyder, A., Kvistborg, P., Makarov, V., Havel, J.J., Lee, W., Yuan, J., Wong, P., Ho, T.S., et al. (2015). Cancer immunology. Mutational landscape determines sensitivity to PD-1 blockade in non-small cell lung cancer. Science *348*, 124–128.

Robert, C., Schachter, J., Long, G.V., Arance, A., Grob, J.J., Mortier, L., Daud, A., Carlino, M.S., McNeil, C., Lotem, M., et al. (2015). Pembrolizumab versus ipilimumab in advanced melanoma. N. Engl. J. Med. *372*, 2521–2532.

Rojas-Sepulveda, D., Tittarelli, A., Gleisner, M.A., Avalos, I., Pereda, C., Gallegos, I., Gonzalez, F.E., Lopez, M.N., Butte, J.M., Roa, J.C., et al. (2018). Tumor lysate-based vaccines: on the road to immunotherapy for gallbladder cancer. Cancer Immunol. Immunother. *67*, 1897–1910.

Rooney, M.S., Shukla, S.A., Wu, C.J., Getz, G., and Hacohen, N. (2015). Molecular and genetic properties of tumors associated with local immune cytolytic activity. Cell *160*, 48–61.

Roufas, C., Chasiotis, D., Makris, A., Efstathiades, C., Dimopoulos, C., and Zaravinos, A. (2018). The expression and prognostic impact of immune cytolytic activity-related markers in human malignancies: a comprehensive meta-analysis. Front. Oncol. *8*, 27.

Saxena, M., Balan, S., Roudko, V., and Bhardwaj, N. (2018). Towards superior dendritic-cell vaccines for cancer therapy. Nat. Biomed. Eng. *2*, 341–346.

Schoenberg, D.R., and Maquat, L.E. (2012). Regulation of cytoplasmic mRNA decay. Nat. Rev. Genet. *13*, 246–259.

Schumacher, T.N., and Schreiber, R.D. (2015). Neoantigens in cancer immunotherapy. Science *348*, 69–74.

Shimizu, K., Iyoda, T., Okada, M., Yamasaki, S., and Fujii, S.I. (2018). Immune suppression and reversal of the suppressive tumor microenvironment. Int. Immunol. *30*, 445–454.

Snyder, A., Makarov, V., Merghoub, T., Yuan, J., Zaretsky, J.M., Desrichard, A., Walsh, L.A., Postow, M.A., Wong, P., Ho, T.S., et al. (2014). Genetic basis for clinical response to CTLA-4 blockade in melanoma. N. Engl. J. Med. *371*, 2189–2199.

Spranger, S., Spaapen, R.M., Zha, Y., Williams, J., Meng, Y., Ha, T.T., and Gajewski, T.F. (2013). Up-regulation of PD-L1, Ido, and T(regs) in the melanoma tumor microenvironment is driven by CD8(+) T cells. Sci. Transl Med. *5*, 200ra116.

Steinman, R.M. (2012). Decisions about dendritic cells: past, present, and future. Annu. Rev. Immunol. *30*, 1–22.

Steinman, R.M., and Banchereau, J. (2007). Taking dendritic cells into medicine. Nature *449*, 419–426.

Straub, M., Drecoll, E., Pfarr, N., Weichert, W., Langer, R., Hapfelmeier, A., Gotz, C., Wolff, K.D., Kolk, A., and Specht, K. (2016). CD274/PD-L1 gene amplification and PD-L1 protein expression are common events in squamous cell carcinoma of the oral cavity. Oncotarget *7*, 12024–12034.

Tanegashima, T., Togashi, Y., Azuma, K., Kawahara, A., Ideguchi, K., Sugiyama, D., Kinoshita, F., Akiba, J., Kashiwagi, E., Takeuchi, A., et al. (2019). Immune suppression by PD-L2 against spontaneous and treatment-related antitumor immunity. Clin. Cancer Res. *25*, 4808–4819.

Tang, H., Liang, Y., Anders, R.A., Taube, J.M., Qiu, X., Mulgaonkar, A., Liu, X., Harrington, S.M., Guo, J., Xin, Y., et al. (2018). PD-L1 on host cells is essential for PD-L1 blockade-mediated tumor regression. J. Clin. Invest. *128*, 580–588.

Tanyi, J.L., Bobisse, S., Ophir, E., Tuyaerts, S., Roberti, A., Genolet, R., Baumgartner, P., Stevenson, B.J., Iseli, C., Dangaj, D., et al. (2018). Personalized cancer vaccine effectively mobilizes antitumor T cell immunity in ovarian cancer. Sci. Transl. Med. *10*, eaao5931.

Topalian, S.L., Drake, C.G., and Pardoll, D.M. (2015). Immune checkpoint blockade: a common denominator approach to cancer therapy. Cancer Cell *27*, 450–461.

Topalian, S.L., Hodi, F.S., Brahmer, J.R., Gettinger, S.N., Smith, D.C., McDermott, D.F., Powderly, J.D., Carvajal, R.D., Sosman, J.A., Atkins, M.B., et al. (2012). Safety, activity, and immune correlates of anti-PD-1 antibody in cancer. N. Engl. J. Med. *366*, 2443–2454.

Topalian, S.L., Taube, J.M., Anders, R.A., and Pardoll, D.M. (2016). Mechanism-driven biomarkers to guide immune checkpoint blockade in cancer therapy. Nat. Rev. Cancer *16*, 275–287.

Tran, E., Robbins, P.F., Lu, Y.C., Prickett, T.D., Gartner, J.J., Jia, L., Pasetto, A., Zheng, Z., Ray, S., Groh, E.M., et al. (2016). T-cell transfer therapy targeting mutant KRAS in cancer. N. Engl. J. Med. *375*, 2255–2262.

Tumeh, P.C., Harview, C.L., Yearley, J.H., Shintaku, I.P., Taylor, E.J., Robert, L., Chmielowski, B., Spasic, M., Henry, G., Ciobanu, V., et al. (2014). PD-1 blockade induces responses by inhibiting adaptive immune resistance. Nature *515*, 568–571.

Turajlic, S., Litchfield, K., Xu, H., Rosenthal, R., McGranahan, N., Reading, J.L., Wong, Y.N.S., Rowan, A., Kanu, N., Al Bakir, M., et al. (2017). Insertion-and-deletion-derived tumour-specific neoantigens and the immunogenic phenotype: a pan-cancer analysis. Lancet Oncol. *18*, 1009–1021.

Wang, X., Yang, L., Huang, F., Zhang, Q., Liu, S., Ma, L., and You, Z. (2017). Inflammatory cytokines IL-17 and TNF-alpha up-regulate PD-L1 expression in human prostate and colon cancer cells. Immunol. Lett. *184*, 7–14.

Wei, S.C., Duffy, C.R., and Allison, J.P. (2018). Fundamental mechanisms of immune checkpoint blockade therapy. Cancer Discov. *8*, 1069–1086.

Wilky, B.A. (2019). Immune checkpoint inhibitors: the linchpins of modern immunotherapy. Immunol. Rev. *290*, 6–23.

Yadav, M., Jhunjhunwala, S., Phung, Q.T., Lupardus, P., Tanguay, J., Bumbaca, S., Franci, C., Cheung, T.K., Fritsche, J., Weinschenk, T., et al. (2014). Predicting immunogenic tumour mutations by combining mass spectrometry and exome sequencing. Nature *515*, 572–576.

Yang, W., Lee, K.W., Srivastava, R.M., Kuo, F., Krishna, C., Chowell, D., Makarov, V., Hoen, D., Dalin, M.G., Wexler, L., et al. (2019). Immunogenic neoantigens derived from gene fusions stimulate T cell responses. Nat. Med. *25*, 767–775.

Zou, W., Wolchok, J.D., and Chen, L. (2016). PD-L1 (B7-H1) and PD-1 pathway blockade for cancer therapy: mechanisms, response biomarkers, and combinations. Sci. Transl. Med. *8*, 328rv324.

iScience, Volume *23*

Supplemental Information

PD-L1 Expression Affects Neoantigen Presentation

Masahiro Okada, Kanako Shimizu, Tomonori Iyoda, Shogo Ueda, Jun Shinga, Yoshiki Mochizuki, Takashi Watanabe, Osamu Ohara, and Shin-ichiro Fujii

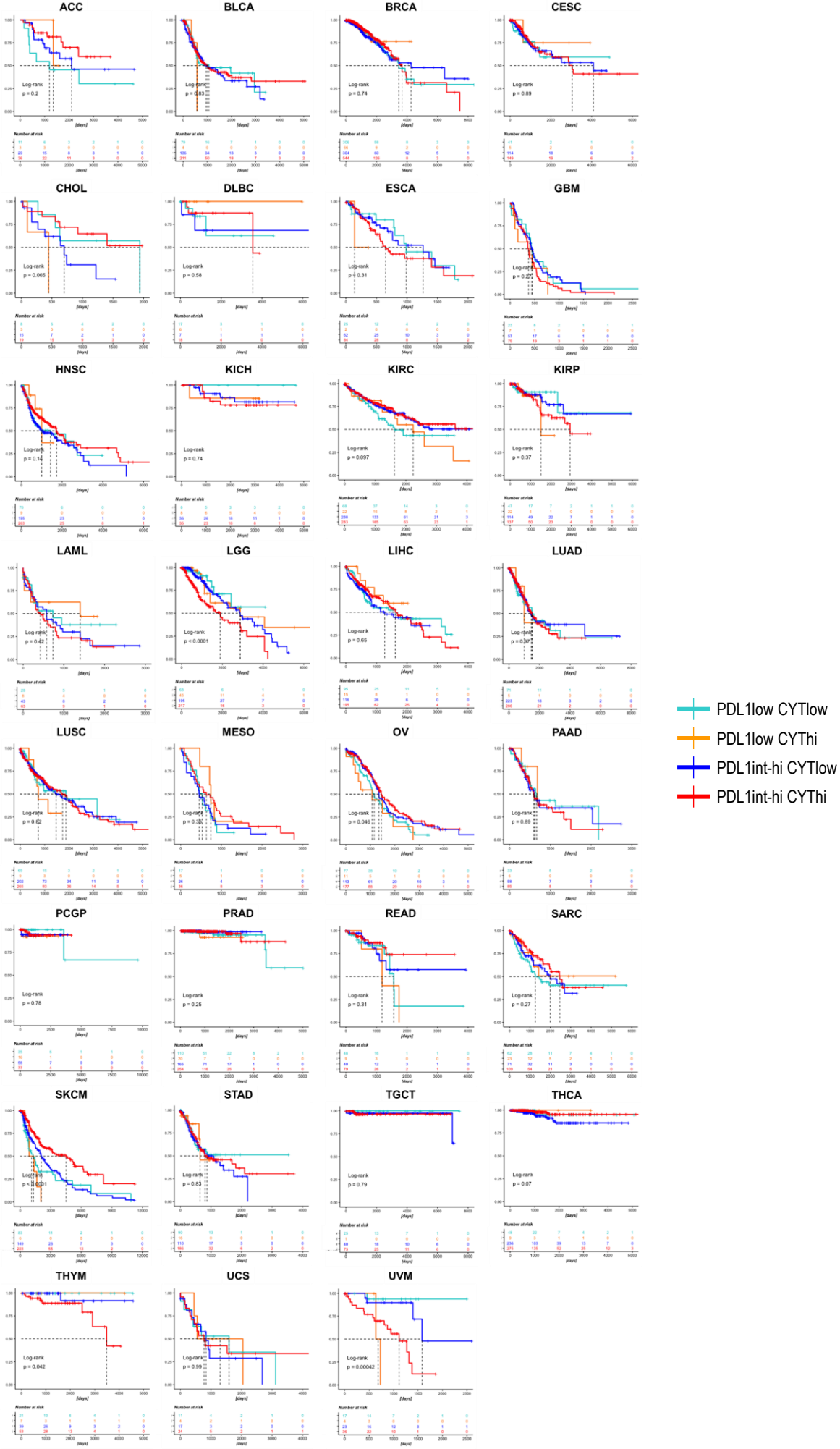

Supplementary Figure 1. TCGA survival analysis focusing on PD-L1 expression with CYT score. Related to Figure 1. Kaplan-Meier survival curves of patients with PD-L1 expression with high versus low CYT score.

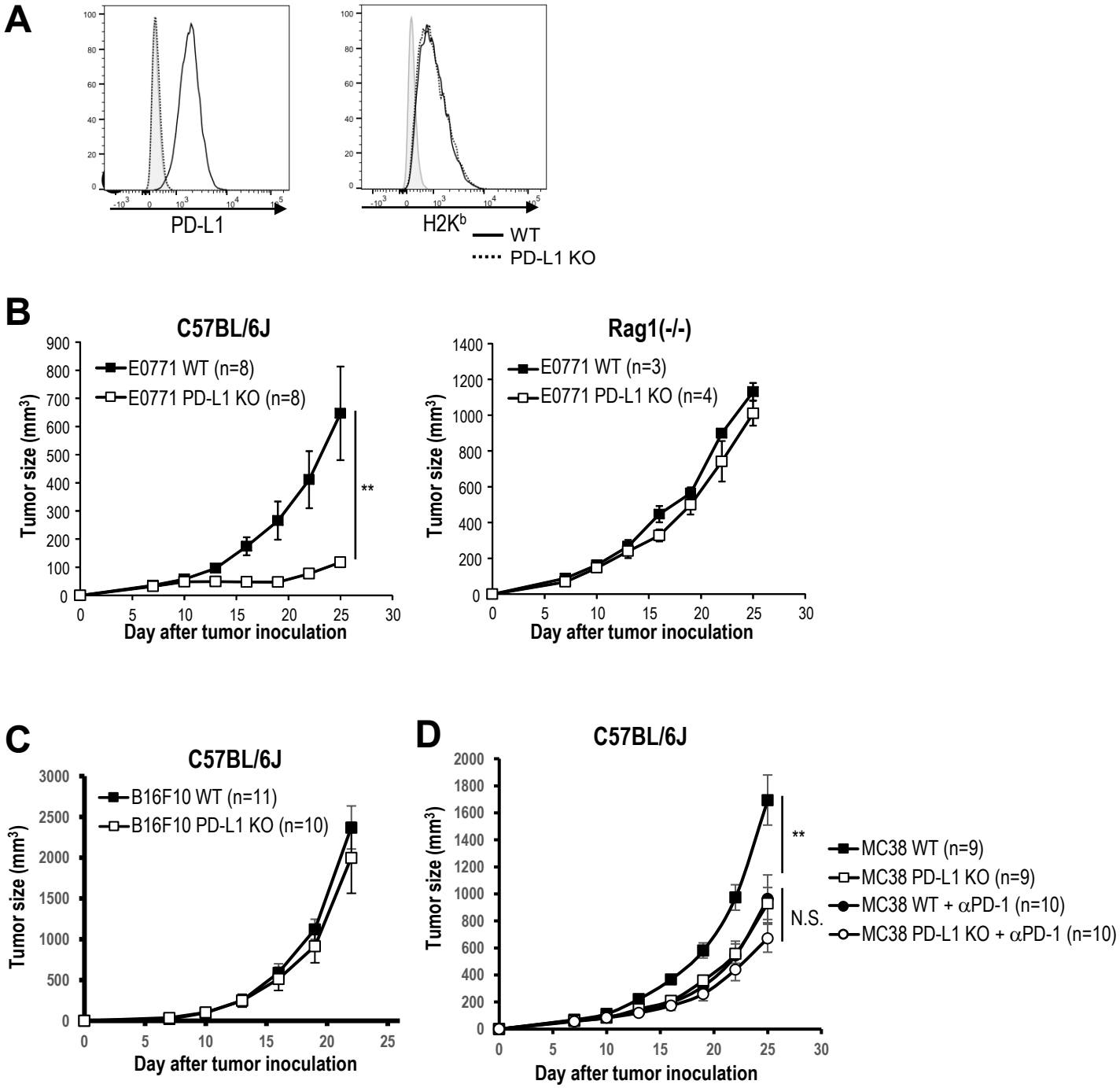

Supplementary Figure 2. Genetic PD-L1 deletion in tumor and effect on antitumor responses. Related to Figure 2.

(A) Flow cytometry analysis of PD-L1 and H-2K^b of MC38-PD-L1-KO cells. **(B)** Tumor growth of E0771 murine breast cancer. C57BL/6J (left) or Rag1$^{-/-}$ (right) mice were subcutaneously (s.c.) injected with 5×10^5 parental or E0771-PD-L1-KO cells, respectively. Tumor growth was monitored at indicated time points by measuring three perpendicular diameters. E0771 and E0771-PD-L1-KO in C57BL/6J mice n = 8/group **$p < 0.01$, in Rag1$^{-/-}$ mice n = 3 and 4/group, respectively; mean ± SEM. **(C)** Tumor growth of B16F10 murine melanoma. Tumor volume was measured every three days from seven days after injection of 1×10^5 parental or B16F10-PD-L1-KO cells in C57BL/6J mice. The values represent mean ± SEM. n = 10 to 11/group. **(D)** Antitumor effect of anti-PD-1 Ab on PD-L1 KO tumor. C57BL/6J mice were s.c. injected with 5×10^5 MC38 or MC38-PD-L1-KO cells and then treated with anti-PD-1 on day 7, 10, and 13. Tumor growth was monitored at indicated time points by measuring three perpendicular diameters. n = 9 to 10/group. Data were analyzed by unpaired Student's t-test, **$p < 0.01$. N.S., non-statistical difference.

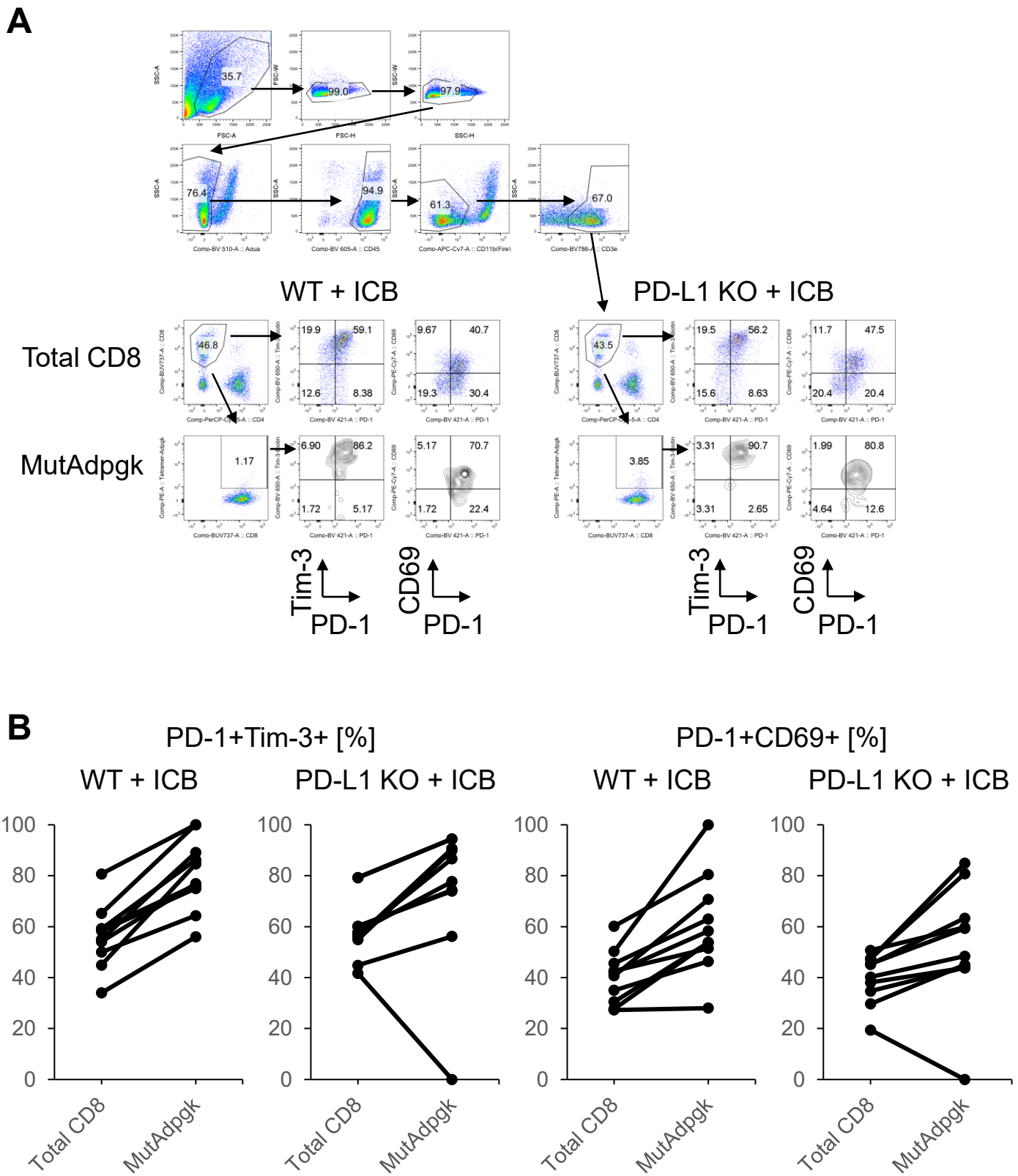

Supplementary Figure 3. Neoantigen specific T cells in tumor infiltrating lymphocytes under ICB therapy. Related to Figure 2.

(A) Gating strategy and representative flowcytometry analysis. **(B)** The percentages of PD-1^{+}Tim-3^{+} or PD-1^{+}CD69^{+} CD8^{+} T cells among total CD8 (non-gated) and MutAdpgk tetramer^{+} cells were plotted. Circles and lines link the respective mice, n=10.

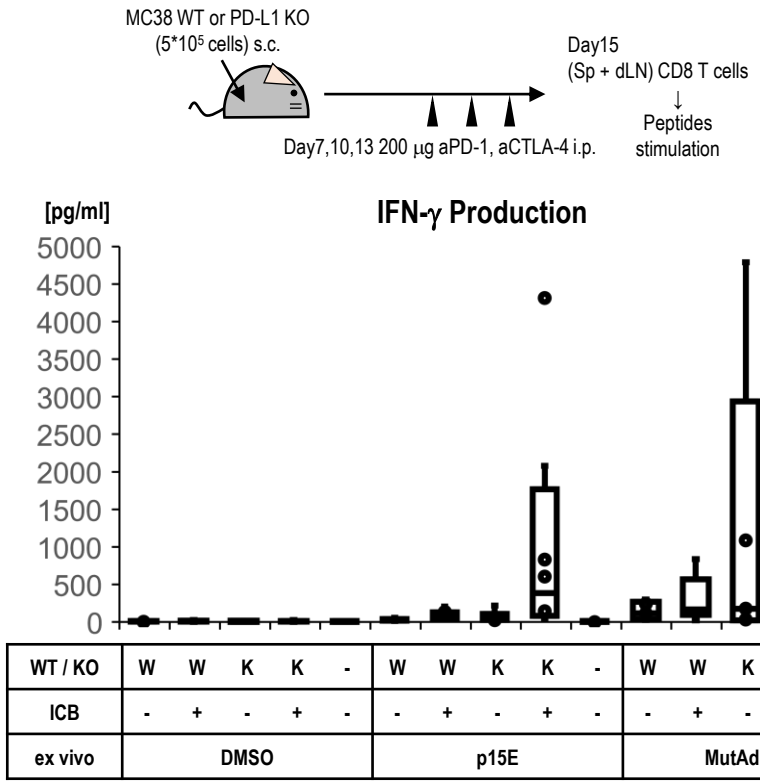

Supplementary Figure 4. Antigen-specific T cell response in ICB-treated mice. Related to Figure 2.
MC38 or MC38-PD-L1-KO tumor-bearing mice were treated with anti-PD-1 and anti-CTLA-4 on day 7, 10, and 13. Fifteen days after tumor inoculation, $CD8^+$ T cells were purified from splenocytes and the tumor draining lymph node, and cocultured with 30 Gy-irradiated splenocytes in the presence or absence of 10 μg/mL p15E or MutAdpgk peptide for 72 h. The culture supernatants were measured for IFN-γ levels by ELISA. Data are pooled from eight or five independent experiments.

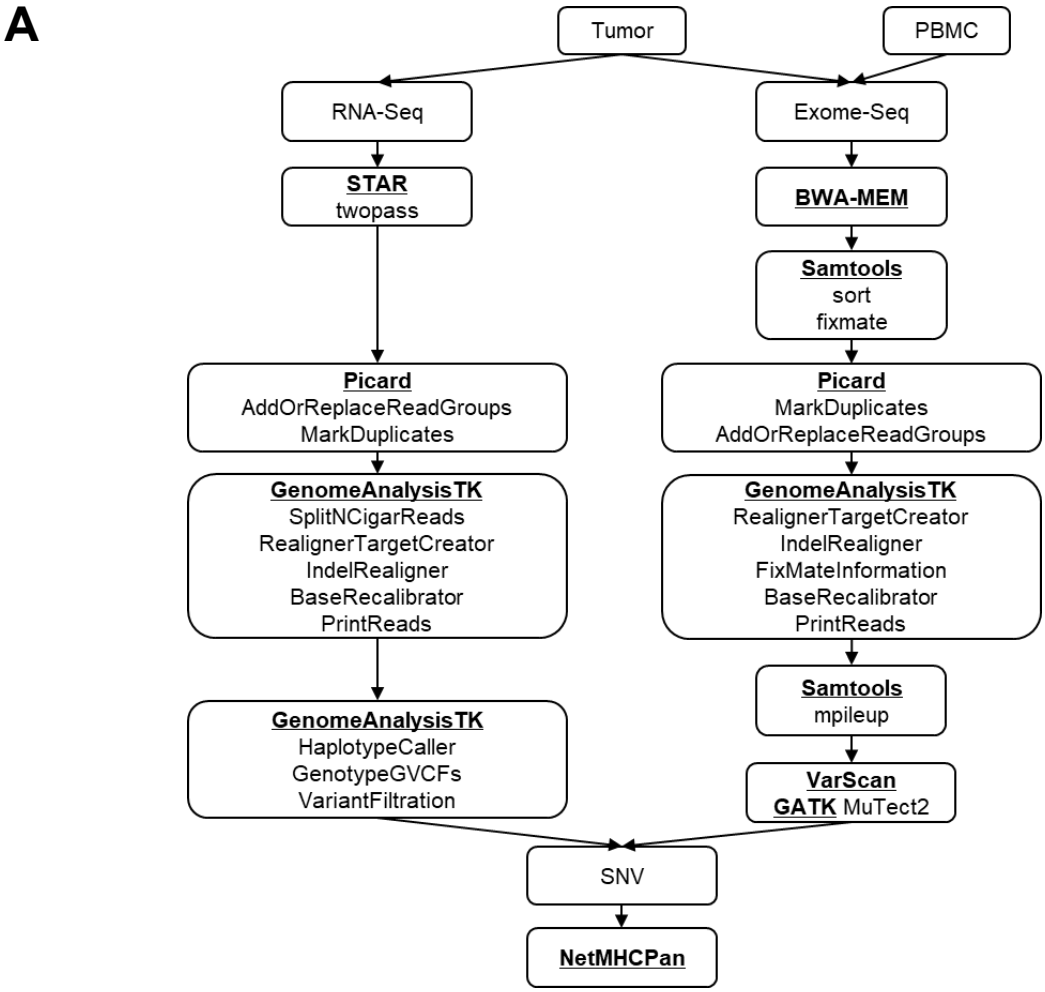

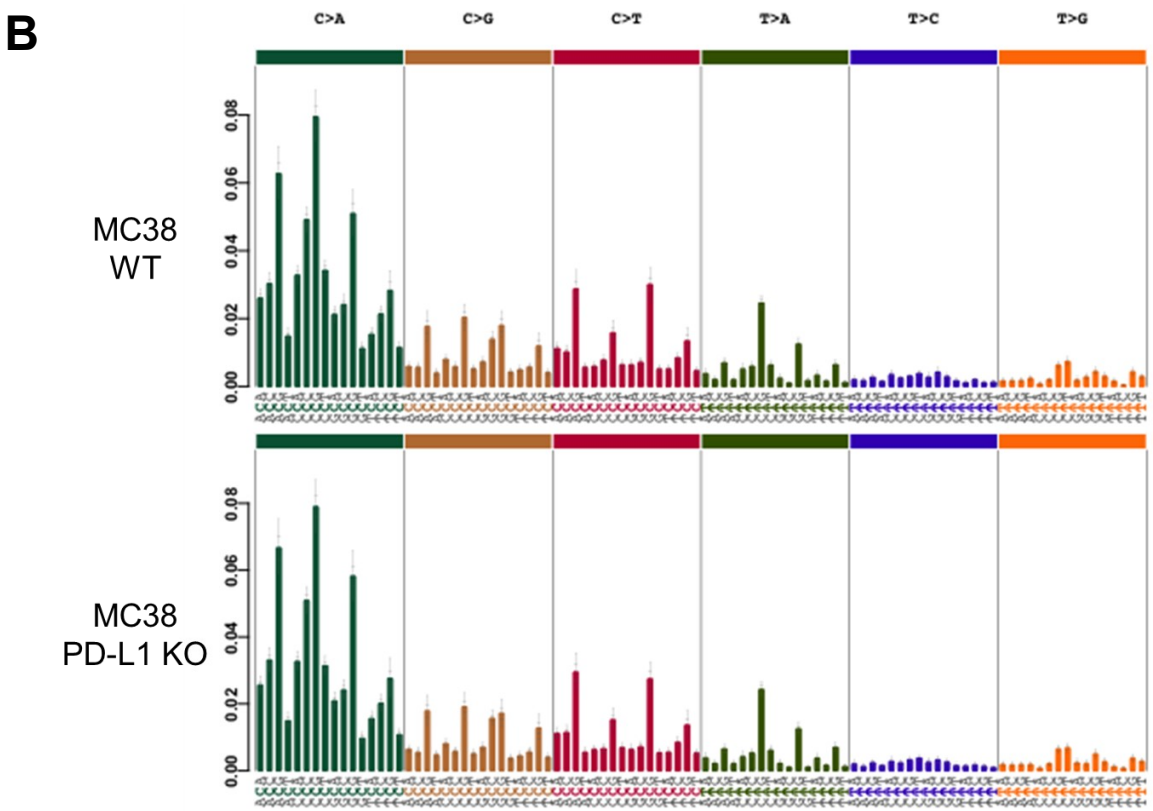

Supplementary Figure 5. Neoantigen identification pipeline. Related to Figure 3.
(A) Mutations in tumors were identified by whole-exome sequence, RNA sequencing, and accompanying bioinformatics approaches using MHC-I-binding algorithms. Reactive peptides sequences and their IC50 values were calculated by NetMHCpan ver3.0. **(B)** Mutation signature analysis of exome sequence from MC38 WT and MC38-PD-L1-KO tumors.

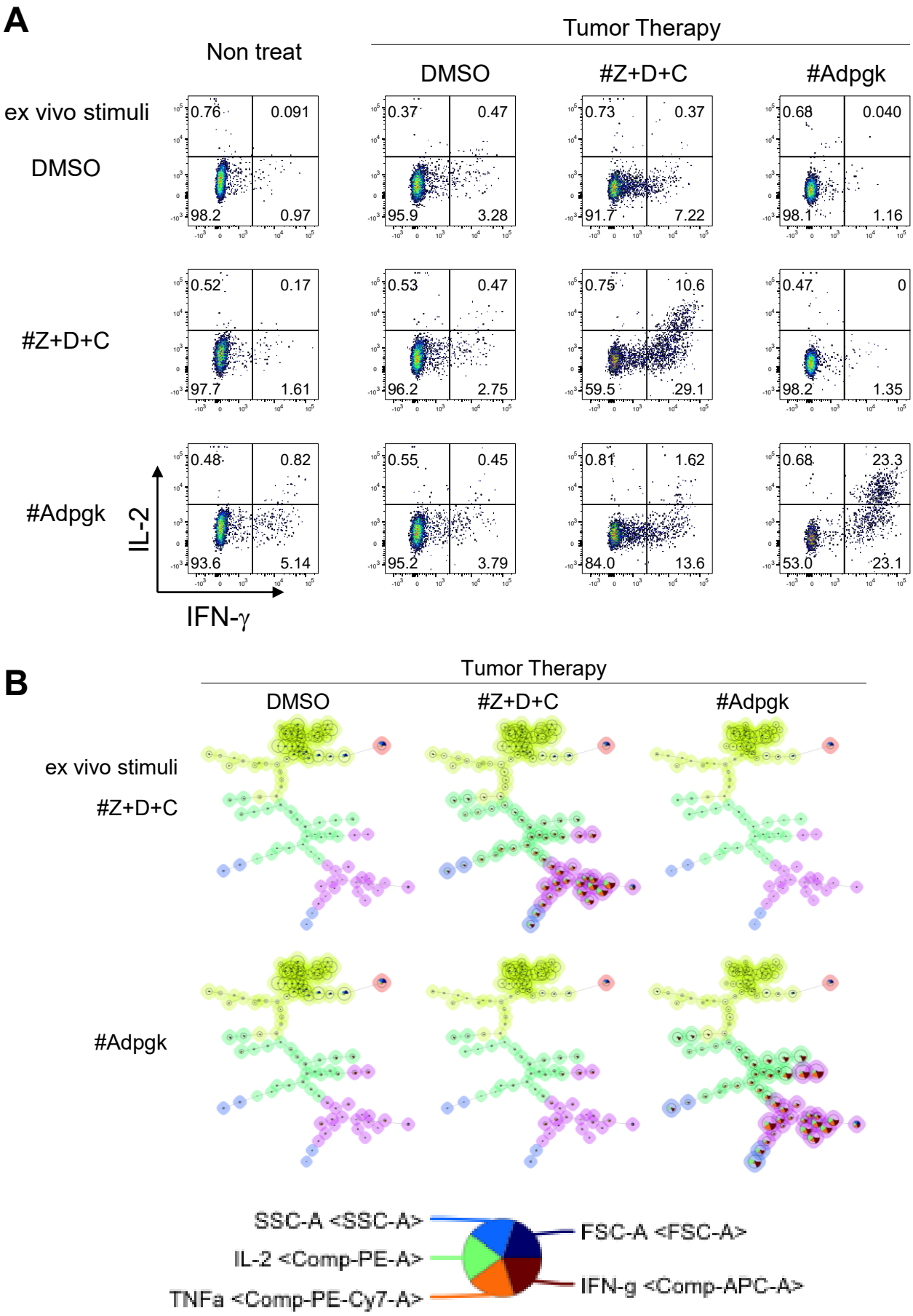

Supplementary Figure 6. Analysis of TIL in mice treated with neoantigen multi-peptides. Related to Figure 6. **(A)** Analysis of TIL in mice treated with neoantigen multi-peptides. TILs from the treated mice were analyzed for cytokine production at day 25. TILs were stimulated by peptides in the presence of anti-CD28 and brefeldin. The frequency of IFN-γ single-producing T cells or IFNγ^{+}IL-2^{+}producing T cells was plotted. Data are pooled from three independent experiments (n = 6). **(B)** FlowSOM analysis representing the multifunctionality of cytokine production in CD8 TILs (IFN-γ^{+}, TNFα^{+} and IL-2^{+}).

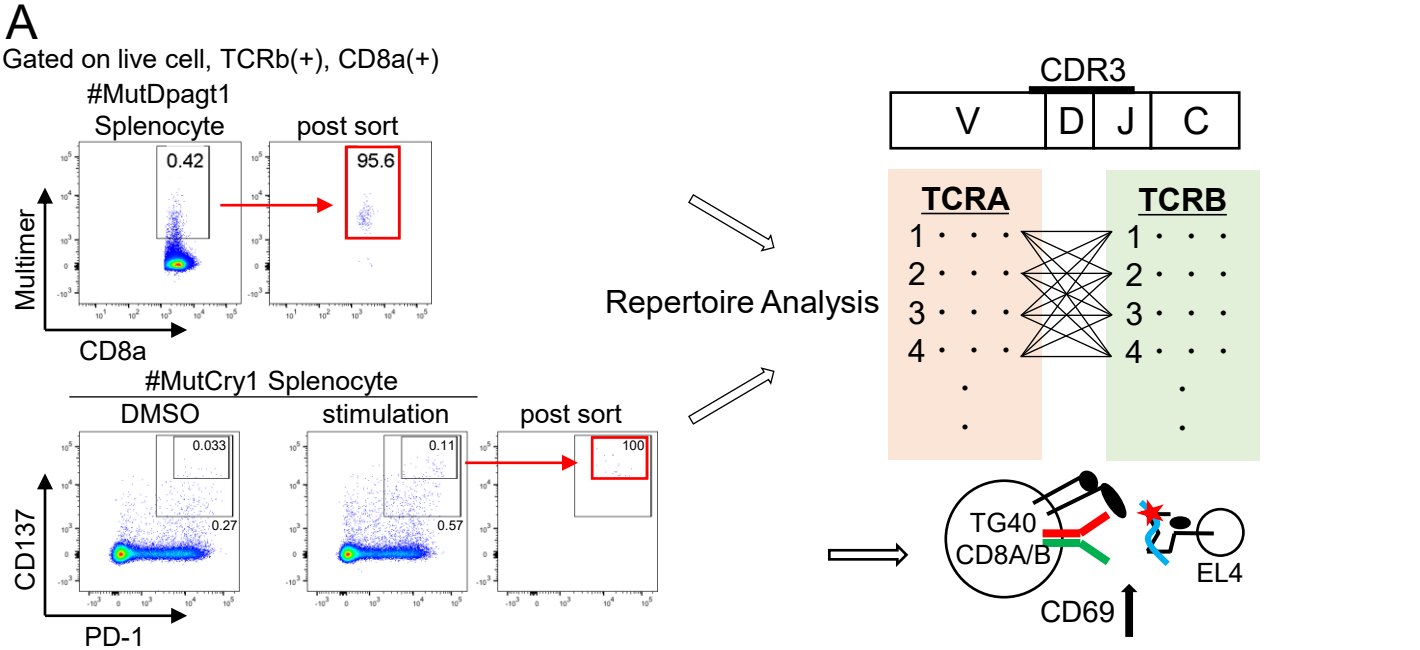

B

Repertoire Top5

#MutDpagt1

TCRA

CDR3 counts	CDR3 Amino Acids Sequence	V gene	D gene	J gene
17964	CATDTNAYKVIF	TRAV8-1*02	-	TRAJ30*01
6854	CATDNMGYKLTF	TRAV8-1*02	-	TRAJ9*01
6088	CAMRDINTGYQNFYF	TRAV16D/DV11*03	-	TRAJ49*01
5484	CAASNMGYKLTF	TRAV7D-2*03	-	TRAJ9*01
4948	CTSETPSPVTLLSTSVQQETGGYKVVF	TRAV7D-2*03	-	TRAJ12*01

TCRB

CDR3 counts	CDR3 Amino Acids Sequence	V gene	D gene	J gene	
15423	CAWRDRGTNTEVFF	TRBV31*01	TRBD1*01	TRBJ1-1*01	
8703	CASSPRTSQNTLYF	TRBV16*01	TRBD2*01	TRBJ2-4*01	
8335	CASSDGGITGQLYF	TRBV13-1*02	TRBD1*01	TRBJ2-2*01	
8067	CASGGTLNTEVFF	TRBV13-2*01	TRBD1*01	TRBJ1-1*01	
6762	CASSLGQLNSDYTF	TRBV12-2*01	TRBD1*01	TRBJ1-2*01	TCR36

#MutCry1

CDR3 counts	CDR3 Amino Acids Sequence	V gene	D gene	J gene
64340	CAASLLNTGNYKYVF	TRAV10*02	-	TRAJ40*01
5262	CAAGGTGYQNFYF	TRAV19*03	-	TRAJ49*01
3521	CALSDPGKLIF	TRAV12N-3*01	-	TRAJ23*01
2657	CALDLMQQGTGSKLSF	TRAV13D-1*02	-	TRAJ58*01
2527	CAVDSGYNKLTF	TRAV7D-2*03	-	TRAJ11*01

CDR3 counts	CDR3 Amino Acids Sequence	V gene	D gene	J gene	
14051	CASSDVEQYF	TRBV13-3*01	TRBD1*01	TRBJ2-7*01	
8496	CASSPDRYEQYF	TRBV16*01	TRBD1*01	TRBJ2-7*01	TCR10
5736	CASSQESWGSSQNTLYF	TRBV2*01	TRBD2*01	TRBJ2-4*01	
5449	CASSQDRGYEQYF	TRBV26*01	TRBD1*01	TRBJ2-7*01	TCR8
4358	CASSPGTFSGNTLYF	TRBV19*01	TRBD1*01	TRBJ1-3*01	

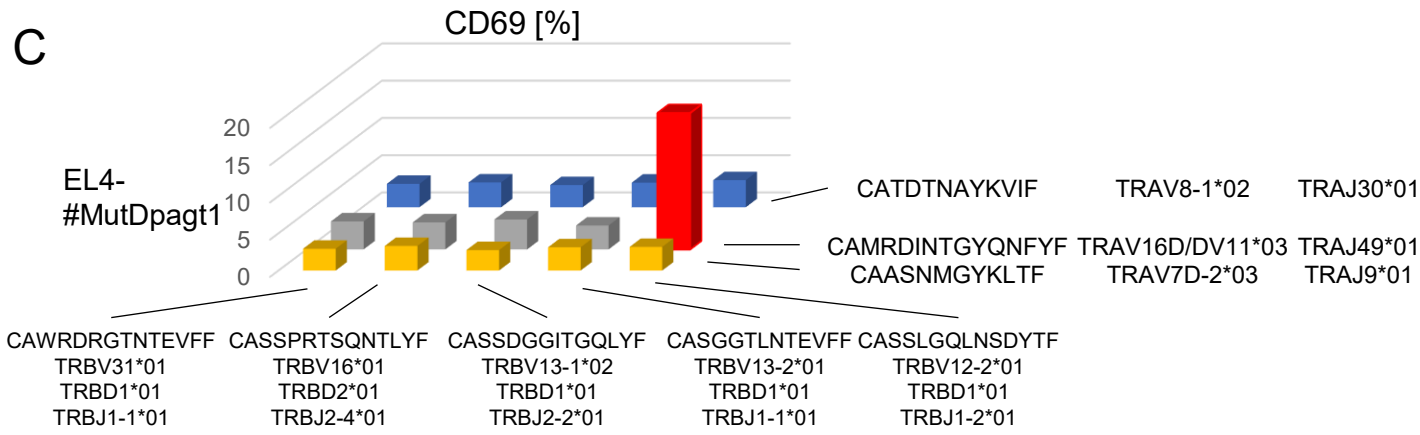

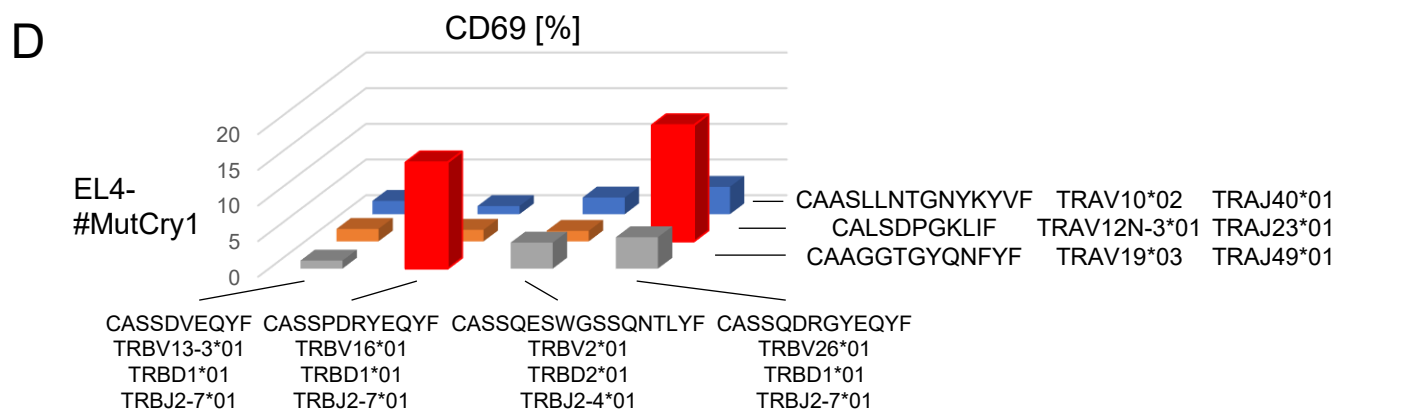

Supplementary Figure 7. Identification of neoantigen-reactive TCR. Related to Figure 7.
(A) Cell sorting of neoantigen-responding CTL. Splenic antigen-specific T cells were isolated as $CD8^+$multimer$^+$ cells for MutDpagt1 and 1-day cultured $CD8^+PD\text{-}1^+CD137^+$ cells for MutCry1 from C57BL/6J mice one week after immunization with neoantigen single peptide (MutDpagt1 or MutCry1) with poly(I:C) and Anti CD40 Abs. Repertoire analyses have been made for each mouse group as shown in the experimental scheme (right). **(B)** Five major TCRα and TCRβ from each group were shown by repertoire analysis. **(C and D)** As shown in the right panel of Fig. S7A, various combinations for TCRα and TCRβ selected from 3–4 major types have been cloned to pMXs-IRES-TdTomato (TCRA) or GFP (TCRB) and transduced to TG40 CD8A/B cells. TG40-bearing TCRA/B (+/+) cells were selected as candidates. Subsequently, these were cocultured with each peptide-pulsed EL4 for 24 h. The percentage of $CD69^+$ cells in TG40 TdTomato/GFP(+/+) cells for MutDpagt1 peptide (C) or MutCry1 peptide (D) is shown. Data are representative of two independent experiments.

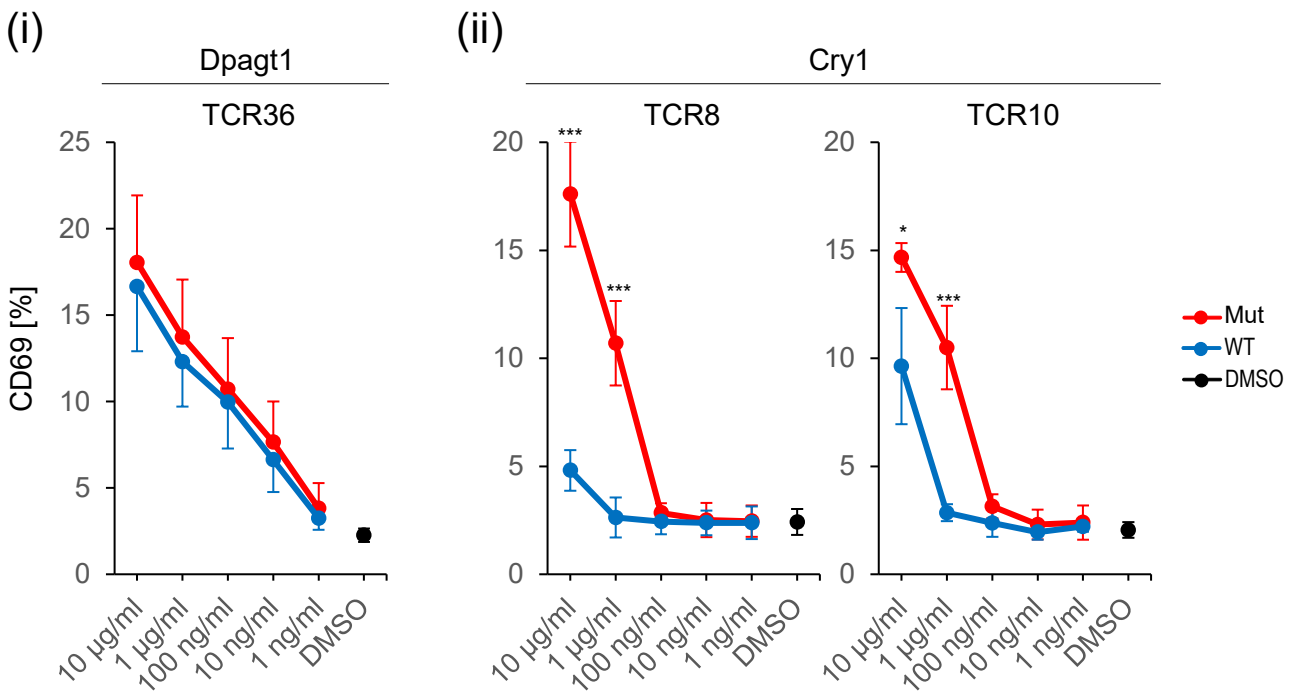

Supplementary Figure 8. Peptide concentration titration of TCRs. Related to Figure 7.
TCR36 (for Dpagt1), TCR8 or TCR10 (for Cry1)-transduced-TG40 cells were cocultured with EL4 in the presence of indicated concentrations of each peptide for 24 h. The percentage of upregulated CD69 of TCR-transduced TG40 cells are shown. Data were pooled from (i) six or (ii) four independent experiments, and the values represent mean ± SD. Data were analyzed by unpaired Student's t-test, *p <0.05, ***p < 0.001.

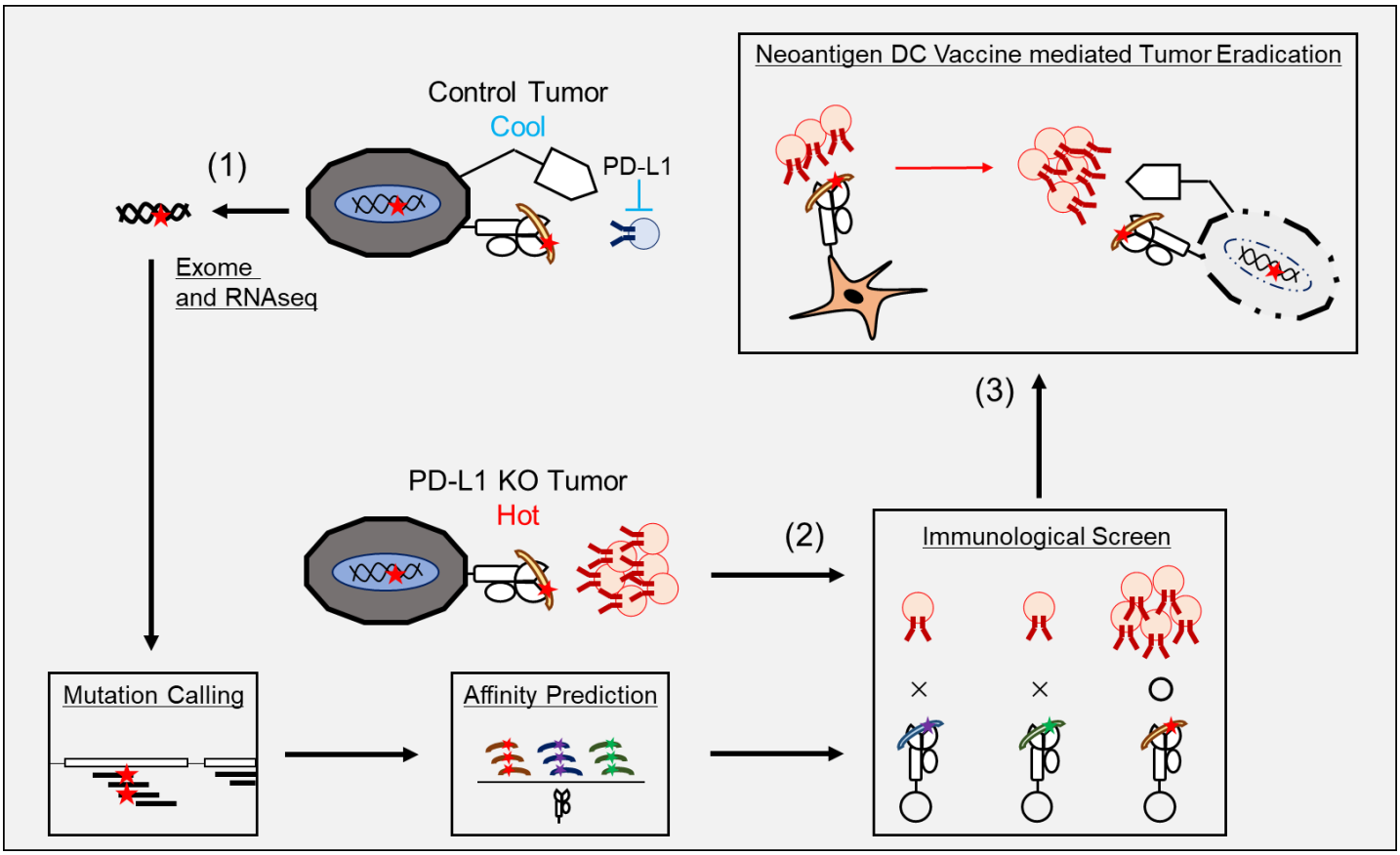

Supplementary Figure 9. Scheme of the study. Related to Figure 2, 3, 5, and 6.
(1) After exome and RNA sequencing, neoantigen candidates were predicted by NetMHCpan. (2) Neoantigens were screened by using activated CTLs from ICB-treated PD-L1 deficient tumor. (3) Vaccination with a mixture of neoantigen-pulsed DCs generated CTLs against PD-L1 positive tumors.

Supplementary Table S1. Neoantigens candidate peptides. Related to Figure 3.

Peptide No	Sequence	IC50(Mut)	Rank(Mut)	Gene Name	Mutation Information	WT Sequence	IC50(WT)
1	KSFHFYCPL	3.3	0.1	Zbtb40	NM_198248 c.G2303C protein-altering (position 768 changed from R to P)	KSFHFYCRL	2.9
2	SNFHFMCAL	6.2	0.1	Kmt2b	NM_001290573 c.G5021T protein-altering (position 1674 changed from R to L)		
3	LSASRYALL	20.7	0.2	Slc12a4	NM_009195 c.G2017T protein-altering (position 673 changed from A to S)		
4	ITIASYIPL	23.4	0.2	Hacd1	NM_013935 c.G648T protein-altering (position 216 changed from M to I)		
5	INFSLQFAL	25	0.2	Pi4kb	NM_001293715 c.G635T protein-altering (position 212 changed from C to F)		
6	RSYQYVMKI	25.3	0.2	Spire1	NM_194355 c.G118T protein-altering (position 40 changed from D to Y)		
7	MSYFLQGTL	26.4	0.2	Copb2	NM_015827 c.A2210C protein-altering (position 737 changed from K to T)		
8	ASYNGFLPV	27.6	0.2	Huwe1	NM_021523 c.C1066A protein-altering (position 356 changed from H to N)		
9	CTFSHLTKL	36.9	0.3	Flrt2	NM_201518 c.G670T protein-altering (position 224 changed from G to C)		
10	KGTLYYYTL	39.5	0.3	Pcsk4	NM_008793 c.C1691A protein-altering (position 564 changed from T to K)		
11	SAMAMFGYM	40.6	0.3	Zbtb8os	NM_025970 c.G167C protein-altering (position 56 changed from C to S)		
12	SSLKSYVQL	42.9	0.3	Ikbkap	NM_026079 c.A943T protein-altering (position 315 changed from T to S)		
13	SAWVPFGGL	43	0.3	Tmem198b	NM_178066 c.G457T protein-altering (position 153 changed from V to F)		
14	ASYSLVAHI	50.7	0.4	Nfe2l2	NM_010902 c.A311T protein-altering (position 104 changed from Q to L)		
15	VQFMSCNLL	51.1	0.4	Taf5l	NM_133966 c.G1717T protein-altering (position 573 changed from A to S)		
16	DVYPFHMIL	52.9	0.4	Gtf3c1	NM_207239 c.A298T protein-altering (position 100 changed from I to F)		
17	KGYRHKVPL	53	0.4	Nsd1	NM_008739 c.A1247T protein-altering (position 416 changed from Q to L)		
18	LMLENYNNL	60.6	0.4	Zfp759	NM_172392 c.G97T protein-altering (position 33 changed from V to L)		
19	SVTVFVNNL	61.7	0.5	Sart3	NM_016926 c.G2126A protein-altering (position 709 changed from S to N)		
20	CVYEHTAVL	62.6	0.5	Herc6	NM_025992 c.G728T protein-altering (position 243 changed from G to V)		
21	RARYFLGNL	69.1	0.5	Dnmt3a	NM_007872 c.G2372T protein-altering (position 791 changed from W to L)		
22	IQPQIYAFL	70.8	0.5	Hace1	NM_172473 c.A2272T protein-altering (position 758 changed from N to Y)		
23	AALTFRRLL	72.4	0.5	Ndufs6	NM_010888 c.T11C protein-altering (position 4 changed from V to A)		
24	KTLTFQGPL	75.2	0.5	Siae	NM_011734 c.A1280C protein-altering (position 427 changed from N to T)		
25	NAFRVYLML	76.9	0.5	Irf2	NM_008391 c.G329T protein-altering (position 110 changed from R to L)		
26	MALSTYYAL	77.7	0.6	Nle1	NM_145431 c.G892T protein-altering (position 298 changed from D to Y)		
27	KNWINYARF	82.7	0.6	Crnkl1	NM_025820 c.G660T protein-altering (position 220 changed from K to N)		
28	FVLESYLNL	83.1	0.6	Rapsn	NM_009023 c.C244G protein-altering (position 82 changed from L to V)		
29	FSLQFALLL	84.4	0.6	Pi4kb	NM_001293715 c.G635T protein-altering (position 212 changed from C to F)		
30	VATINFRRL	86.9	0.6	N4bp2l2	NM_201369 c.G194T protein-altering (position 65 changed from R to L)		
31	FSLSFQHPV	93.2	0.6	Med1	NM_013634 c.G1309T protein-altering (position 437 changed from V to L)		
32	SYIPLFPHL	94.5	0.6	Hacd2	NM_023587 c.G693T protein-altering (position 231 changed from Q to H)		
33	IVAKLIAPL	96.8	0.6	Gcn1l1	NM_172719 c.G4039C protein-altering (position 1347 changed from A to P)		
34	HSFVYSVGF	97.9	0.6	Srebf2	NM_033218 c.G2512T protein-altering (position 838 changed from D to Y)		
35	QIYAFLQGF	108.7	0.6	Hace1	NM_172473 c.A2272T protein-altering (position 758 changed from N to Y)		
36	ASIIVFNLL	118.9	0.6	Dpagt1	NM_007875 c.G637T protein-altering (position 213 changed from V to L)	ASIIVFNLV	609.4
37	SILNWRTKL	142.4	0.7	Ftsj3	NM_025310 c.C922A protein-altering (position 308 changed from L to I)		
38	SAIRSYQYV	146.2	0.7	Spire1	NM_194355 c.G118T protein-altering (position 40 changed from D to Y)		
39	VSRHHRALL	149.5	0.7	Zzef1	NM_001045536 c.G232C protein-altering (position 78 changed from G to R)		
40	YVWGRYDFL	151.4	0.7	Rnpep	NM_145417 c.G864T protein-altering (position 288 changed from L to F)		
41	VIYSECLRV	162.9	0.8	Atm	NM_007499 c.G7036T protein-altering (position 2346 changed from A to S)		
42	QFFHCYCPL	164.7	0.8	Cry1	NM_007771 c.G1246T protein-altering (position 416 changed from V to L)	QFFHCYCPV	781.2
43	IAECTFSHL	176.5	0.8	Flrt2	NM_201518 c.G670T protein-altering (position 224 changed from G to C)		
44	MMKYYYESV	179.6	0.9	Carnmt1	NM_026120 c.G1172C protein-altering (position 391 changed from C to S)		
45	AAALTFRRL	191.5	0.9	Ndufs6	NM_010888 c.T11C protein-altering (position 4 changed from V to A)		
46	SLLEHMSLL	197.4	0.9	Zbtb24	NM_153398 c.A1112T protein-altering (position 371 changed from H to L)		
47	SCRTFLSPL	199.6	0.9	Entpd7	NM_053103 c.G1155C protein-altering (position 385 changed from L to F)		
48	SHYVLYGLI	78.9	0.6	Psmd2	NM_134101 c.G2464A protein-altering (position 822 changed from V to I)		
49	VLYGLIAAM	144.2	0.7	Psmd2	NM_134101 c.G2464A protein-altering (position 822 changed from V to I)		

Transparent Methods

EXPERIMENTAL MODEL AND SUBJECT DETAILS

Mice

Pathogen-free, 6–8 week old C57BL/6J female mice were purchased from Charles River Japan, and Rag1 knockout mice were purchased from The Jackson Laboratory. All mice were maintained under specific pathogen-free conditions. All mice experiments were approved by and performed in compliance with Institutional Animal Care and Use Committee of RIKEN Yokohama Branch.

Reagents

InVivoMAb Anti-mouse PD-1 (RMP1.14) and Anti-mouse CTLA-4 (9D9) were purchased from BioXCell (West Lebanon, NH, USA). H2Kb MuLV p15E peptide (KSPWFTTL) was purchased from MBL (Aichi, Japan).

Flow cytometry

The following monoclonal antibodies (mAbs) were purchased from BD Bioscience, BioLegend, eBioscience, or MBL: anti-CD274 (10F.9G2), anti-H2-K^b (AF6-88.5), anti-CD4 (GK1.5), anti-TCRβ (H57-597), anti-CD8a (53-6.7), anti-TNF-α (MP6-XT22), anti-IL-2 (JES6-5H4), anti-IFN-γ (XMG1.2), anti-CD44 (IM7), anti-CD137 (17B5), anti-CD62L (MEL-14), anti-PD-1 (29F.1A12), anti-CD8 (KT-15), anti-CD3e (145-2C11), anti-CD45 (30-F11), anti-CD8b (YTS156.7.7), anti-CD69 (H1.2F3), anti-CD11b (M1/70), anti-CD366 (RMT3-23), anti-Ly-6C (HK1.4), anti-CD24 (M1/69), anti-Siglec-F (E50-2440), anti-F4/80 (BM8), anti-I-A/I-E (M5/114.15.2), anti-CD103 (2E7), anti-Ly-6G (1A8), anti-CD11c (HL3), anti-CD19 (1D3), anti-CD25 (PC61), anti-NK-1.1 (PK136), anti-CD4 (RM4-5), and anti-FOXP3 (FJK-

16s). H2-D^b Adpgk neoepitope tetramer and H2-K^b Zbtb40 and Dpagt1 neoepitope multimers were purchased from MBL and Immudex (Copenhagen, Denmark), respectively.

Cell culture

MC38 (a kind gift from Dr. MT Lotze, University of Pittsburgh), HEK293T cells and B16F10 cells from ATCC were maintained in Dulbecco's Modified Eagle Medium (DMEM, 4500 mg/L glucose) supplemented with 10% fetal bovine serum (FBS) and 1% penicillin/streptomycin (Gibco). E0771 cells from CH3 BioSystems, EL-4 cells (a kind gift from Dr. Steinman, The Rockefeller University), and TG40 cells expressing CD8A and CD8B (a kind gift from Dr. T Saito, RIKEN) (Yokosuka et al., 2002) were cultured in Roswell Park Memorial Institute (RPMI) 1640 medium supplemented with 10% FBS, 55 μM 2-ME, and 1% penicillin/streptomycin. TG40 cells were constantly sorted to maintain CD8A and CD8B expression at > 95%. Primary T cells were cultured in RPMI-1640 medium supplemented with 10% FBS, 55 μM 2-ME, 1% penicillin/streptomycin, 1% non-essential amino acid solution, and 2 mM L-glutamine. Bone marrow cells were cultured in RPMI-1640 medium supplemented with 5% FBS, 55 μM 2-ME, 1% penicillin/streptomycin, and 1 mM HEPES with GM-CSF Sup derived from J558L-GM-CSF. All cells were cultured in a humid, 5% CO_2, 37°C incubator.

Bone marrow-derived dendritic cell culture and vaccination

Bone marrow-derived DCs were generated in the presence of GM-CSF and matured using LPS on day 6 as previously described (Shimizu et al., 2006). On the following day, mature DCs were harvested and pulsed with 10 μg/mL of indicated peptides for 2 h. After washing with PBS, peptide-pulsed DCs (1×10^6) were intravenously injected for vaccination.

MC38 transplantation mouse model

Briefly, 6 to 10-week-old female mice were shaved on the right flank, and MC38 (1 or 5×10^5 cells) was subcutaneously injected. Tumor volume, calculated as 0.52 × Length × Width × Height [mm^3], was measured at day 7 and every three days. For ICB treatment, 200 μg anti-mouse PD-1 (RMP1.14) and 200 μg anti-mouse CTLA-4 (9D9) were intraperitoneally injected on day 7, 10, and 13. For the CD4 or CD8 T cell-depletion, 250 μg anti-mouse CD4 (GK1.5) or anti-mouse CD8 (53-6.7) were injected intraperitoneally on day -2, 0, 2 and 4, and moreover every 3 to 4 days.

Poly(I:C), anti-CD40 antibody and peptide immunization

10 μg PolyI:C, 30 μg anti-CD40 antibody (1C10) (BioLegend), and 100 μg indicated peptides dissolved in 200 μL PBS were intravenously injected for vaccination (33.3 μg each of peptide #1, #36, and #42 immunization was used) into 6 to 10-week-old female mice. Or 50 μg PolyI:C, 50 μg anti-CD40 antibody, and 100 μg peptide were used for immunization into tumor bearing mice in TCR isolation experiments. 1 week after immunization, splenocytes were further analyzed for multimer staining, intracellular cytokine staining after 6 h culture in the presence of GolgiPlug (BD Bioscience), and activation marker staining and ELISA after 24 h culture with 10 μg/ml peptide.

Neoantigen prediction

Missense mutation-containing amino acid sequences, positioned at 9 in 17 aa, near the first Met, or near the stop codon, were investigated for their potential loading to MHC class I H2-K^b using the NetMHCpan (version 3.0) (Nielsen and Andreatta, 2016) algorithm provided by Immune Epitope DataBase and Analysis Resource (http://tools.iedb.org/mhci/). Predicted peptide length was set as 9 mer. Top 48 candidate peptides (IC50 < 200 nM) were narrowed

down for further biological investigation. Candidate peptides (Table S1) and MutAdpgk (ASMTNMELM) were synthesized (purity > 90%) by GenScript Japan (Tokyo, Japan).

Flow cytometry

Fixable Violet or Aqua Dead Cell stain kit (Invitrogen) was used to eliminate dead cells. Cytokine expression by CD8 T cells was determined using a protocol for intracellular cytokine staining (Shimizu and Fujii, 2009). Briefly, splenic cells were incubated in the presence of Golgi Plug (BD Bioscience) for 6 h with or without 10 μg/mL indicated peptide, followed by incubation with antibodies to the surface markers. Isolated TILs (~1 × 10^6 cells/200 μL) were seeded in 96-well round bottom plates and stimulated with 10 μg/mL indicated peptides and soluble 2 μg/mL anti-CD28 (clone 53.67) (BioLegend) in the presence of GolgiPlug for 6 h. Each 3.3 μg/mL #1, #36, and #42 peptide was used for mixed peptides stimulation. Cells were treated with the anti-mouse CD16/32 antibody (clone 93) (BioLegend) and then stained using cell surface antibodies. Subsequently, the cells were permeabilized in Cytofix-Cytoperm Plus (BD Biosciences) and stained with anti-IFN-γ, -TNF-α, and -IL-2 mAb. Splenocytes (0.5~1 × 10^7 cells) or TILs were treated with anti-mouse CD16/32 antibody in a 50 μL volume, followed by addition of ~10 μL volume of MHC dextramer or MutAdpgk tetramer.

CD69 upregulation assays

TCR retroviruses were transduced into TG40 CD8A/B cells in the presence of 5 μg/mL polybrene (Nacalai) by centrifugation at 2300 rpm for 90 min at 35°C. Further, 2–3 × 10^4 Bulk TG40 cells were cocultured with the same number of EL-4 in the presence or absence of 10 μg/mL corresponding peptides for 24 h in a 96-well flat plate. CD69 upregulation in $TdTomato^+GFP^+$ or GFP^+ cells was analyzed by FACS.

TCR-T assay

MACS-sorted 2×10^5 CD8 T cells were cultured with 2×10^5 mouse CD3/28 beads using the Treg expansion kit (Miltenyi Biotec) and 100 U Immunace (recombinant human IL-2) (Shionogi, Osaka, Japan) in a 24-well plate. Two days after stimulation, TCR retroviruses were transduced into cells in the presence of 6 μg/mL polybrene by centrifugation at 2300 rpm for 90 min at 35°C. On the following day, the cells were harvested and resuspended in fresh medium containing IL-2 after magnetic removal of CD3/28 beads. Two days after transduction, $CD8^+GFP^+$ cells were sorted. Approximately 5×10^4 CD8 T cells were cocultured with 1×10^4 MC38 cells with or without 10 μg/mL peptide for 48 h in the presence of 100 U IL-2 in 96-well flat plates. Culture supernatants were harvested and subjected to IFN-γ ELISA.

TCGA Analysis

Gene expression data (FPKM values) were downloaded from the TCGA GDC portal site (https://portal.gdc.cancer.gov/repository) using gdc-rnaseq-tool (https://github.com/cpreid2/gdc-rnaseq-tool), and clinical data were obtained using R package “TCGAbiolinksGUI" (Silva et al., 2018) on October 2019. FPKM values were converted to TPM values. CYT scores were defined as geomeans of GZMA and PRF1. Overall survival of sub-grouped patients was parsed by R package “survival" and R package “survminer".

Establishment of PD-L1 Knockout cells

gRNA targeting mouse PD-L1 (chr19:29373571-93) expression vector was generated by annealing of oligonucleotides, followed by ligation into BsmBI and BamHI-restricted sites of pCas-Guide-EF1a-GFP (OriGene #GE100018). Primers (forward; gatcgGGCTCCAAAGGACTTGTACGg and reverse;

aaaacCGTACAAGTCCTTTGGAGCCc) were used for construction. CRISPR-Cas9 #PD-L1 vector was transfected into MC38, B16F10, and E0771 cells using the Lipofectamine Plus Reagent and LTX reagent, followed by a medium change to remove the transfection reagents. Three days after transfection, GFP^+ cells were sorted using ARIA3 (BD Biosciences, San Jose, CA, USA) and further cultured. Seven days after transfection, cells were detached using Accutase (Nacalai). Following, PD-L1(-)GFP(-) cells were sorted and further expanded. Several sorting was performed consecutively after expansion to yield completely PD-L1 knockout cells.

IFN-γ ELISA and ELISPOT assay

CD8 T cells were positively selected by mouse CD8a (Ly-2) MicroBeads (Miltenyi Biotec) and MACS LS column. The purity was almost > 90%. For ELISA analysis, 2×10^5 CD8 T cells were MACS purified from the spleen and draining lymph node in tumor-bearing mice, and 2×10^5 30 Gy-irradiated splenocytes were cocultured in the presence of 10 μg/mL peptides in a total volume of 200 μL/well for 72 h. Following, the culture supernatants were harvested and stocked. Technical-duplicate wells were prepared for assays, except the neoantigen peptides screen. IFN-γ production in the frozen and thawed samples were examined using Mouse IFN-γ Duo Set ELISA (R&D systems, Minneapolis, MN, USA) and High Binding Coaster Assay Plates (Corning). ELISPOT assays for antigen-specific IFN-γ secreting cells were performed on 96-well filtration plates (Merck Millipore) coated with rat anti-mouse IFN-γ capture antibody at 10 μg/mL (BD Biosciences R4-6A2) as previously described (Shimizu et al., 2007). Splenic and lymph node CD8 T cells were isolated from immunized mice or naïve mice using $CD8^+$ MACS Beads. Further, 5×10^5 CD8 T cells were cocultured with 3×10^5 irradiated splenic cells pulsed with the indicated peptides for 40–48 h. Biotinylated anti-mouse IFN-γ detection antibody was added at 2 μg/mL (BD Biosciences,

XMG1.2) for 2 h, and spots were developed with Streptavidin-HRP (BD Biosciences) for 1 h and stable DAB substrate (FALMA, Tokyo, Japan). Finally, cells were counted microscopically.

Exome-seq and RNA-seq

MC38 WT and PD-L1 KO tumor tissues were resected and divided into two samples for exome-seq and RNA-seq, then snap frozen in liquid nitrogen. Whole blood was sampled with heparin, and centrifuged PBMCs were prepared for normal tissues. For exome-seq, genomic DNA was extracted using the Wizard Genomic DNA Purification Kit (Promega). DNA was sheared by Covaris (Covaris), and the exome was captured using the SureSelectXT mouse all exon system (Agilent Technologies, 5190-4641) for library preparation. For RNA-seq, RNA was extracted using the Trizol LS Reagent and isolated with chloroform. Following, RNA was precipitated with glycogen and isopropanol, followed by 75% ethanol wash. mRNA was retrieved with oligo dT beads. The RNA sequencing library was prepared using the SureSelect Strand-Specific RNA Library Prep kit (Agilent Technologies, G9691A). Library preparation and pair-end sequencing (100 cycles for RNA sequencing;125 cycles for exome sequencing) on a HiSeq2500 (Illumina) were performed by the Kazusa DNA Research Institute.

Variant calling

Exome-seq data were mapped onto the reference mouse genome (MM9) by BWA-MEM (Li, 2013; Vasimuddin et al., 2019) with default parameters. After removal of unmapped reads, the rest of sequence reads were sorted with a Samtools (Li et al., 2009; Li, 2011). Subsequently, the bam files were processed for removal of PCR duplicates (Picard) and indel realignment, followed by base recalibration referring SNP (number) (GATK) (McKenna et al., 2010). Mutect2 (https://software.broadinstitute.org/ gatk/ documentation/tooldocs/3.8-

0/org_broadinstitute_gatk_tools_walkers_cancer_m2_ MuTect2.php) and VarScan 2 (Koboldt et al., 2012) were used to detect tumor specific variants in comparison with those found by germline blood exome-seq and the variants detected by both of the detection tools were taken as candidate ones in this study. Mutation signature analysis was performed by signeR. RNA-seq data were mapped onto mouse reference genome (MM9) by STAR with two-pass alignment (Dobin et al., 2013). The bam files were processed for removal of PCR duplicates (Picard) and inaccurate spliced reads, and indel realignment, followed by base recalibration referring SNP (number) (GATK). Variants were called using GATK HaplotypeCaller.

T cell receptor repertoire assay

Total RNA was extracted from TrizolLS lysed highly sorted multimer^{+}CD8^{+} T cells or peptide stimulated PD-1^{+}CD137^{+}CD8^{+} T cells and reverse transcribed for first-strand cDNA synthesis using a SMARTer Mouse TCR a/b Profiling kit (Clontech). Both universal mix primer and primers specific for the T cell receptor constant region sequence were used for second-strand amplifications, resulting in TCR PCR products of high purity, which were then submitted for high-throughput DNA sequencing using an Illumina Miseq sequencing system. The sequencing was performed with the paired end (Read1: 300 nt, Read2: 300 nt) using the MiSeq Reagent Kit v3 (MS-102-3003, Illumina). All reads of the TCRα and TCRβ repertoire sequence were analyzed using LymAnalyzer ver1.2.2 (Yu et al., 2016), or randomly extracted 1000 sequences of TCRβ by SeqKit (Shen et al., 2016) were parsed by TCRdist (Dash et al., 2017).

TCR expression vector cloning

The VDJ regions were amplified by PCR using the second PCR products described above as templates, and cloned together with the corresponding C region into pMXs retroviral vectors.

Peptide-reactive pairs of TCRA and TCRB were concatenated with Furin (RAKR)-SGSG-P2A and cloned into pMXs-IRES-GFP. Site-directed mutagenesis was carried out by PCR.

Retrovirus production

pMXs and pCL-Eco were co-transfected into HEK293T cells using FuGene6 (Promega), followed by a medium change to remove the transfection reagents. Virus-containing medium was harvested after 48 h.

WST-1 Assay

Briefly, 1×10^3 MC38 cells were seeded in triplicated well on each 96-well plate before using the Premix WST-1 Cell Proliferation Assay System (Takara Bio Inc, Shiga, Japan) at 24, 48, and 72 h culture. Absorbance was measured after a 1-h incubation. Relative proliferation on day 1 was monitored.

Statistical analysis

Statistical analysis was performed using Microsoft Excel, R, and StatMate. Unpaired student's t-test were used for two experimental groups' comparison. One-way ANOVA followed by Tukey-test were used for multiple experimental groups' comparison. Kaplan-Meier survival curves were analyzed by the log-rank test. P values under 0.05 were considered statistically significant and indicated with *, $p < 0.05$; **, $p < 0.01$; ***, $p < 0.0001$.

KEY RESOURCES TABLE

REAGENT or RESOURCE	SOURCE	IDENTIFIER
Antibodies (for FACS, ELISPOT, Biological Analysis)		
Biotin Mouse IgG1, κ Isotype Ctrl Antibody, MOPC-21	BioLegend	Cat# 400104, RRID:AB_326427
Biotin anti-mouse CD274 (B7-H1, PD-L1) antibody, 10F.9G2	BioLegend	Cat# 124306, RRID:AB_961220
eBioscience™ Streptavidin PE Conjugate	eBioscience™,	Cat# 12-4317-87
Mouse IgG1, kappa Isotype Control, PE Conjugated, Clone MOPC-21 antibody	BioLegend	Cat# 400113, RRID:AB_326435
PE anti-mouse H-2Kb antibody, AF6-88.5	BioLegend	Cat# 116508, RRID:AB_313735
PerCP anti-mouse CD4 antibody, GK1.5	BioLegend	Cat# 100432, RRID:AB_893323
PE/Cy7 anti-mouse TCRb chain antibody, H57-597	BioLegend	Cat# 109222, RRID:AB_893625
APC/Cyanine7 anti-mouse CD8a antibody, 53-6.7	BioLegend	Cat# 100714, RRID:AB_312753
Alexa Fluor® 488 anti-mouse TNF-a antibody, MP6-XT22	BioLegend	Cat# 506313, RRID:AB_493328
PE anti-mouse IL-2 antibody, JES6-5H4	BioLegend	Cat# 503808, RRID:AB_315302
Brilliant Violet 421™ anti-mouse IFN-g antibody, XMG1.2	BioLegend	Cat# 505830, RRID:AB_2563105
Rat Anti-CD44 Monoclonal Antibody, FITC Conjugated, Clone IM7	BD Biosciences	Cat# 553133, RRID:AB_2076224
PE anti-mouse CD137 antibody, 17B5	BioLegend	Cat# 106106, RRID:AB_2287565
CD62L (L-Selectin) Monoclonal Antibody (MEL-14), APC, eBioscience™	Invitrogen	Cat# 17-0621-82, RRID:AB_469410
Brilliant Violet 421™ anti-mouse CD279 (PD-1) antibody, 29F.1A12	BioLegend	Cat# 135221, RRID:AB_2562568
Anti-CD8 (Mouse) mAb-FITC, KT15	MBL	Cat# D271-4, RRID:AB_10597265
FITC anti-mouse CD8a antibody, 53-6.7	BioLegend	Cat# 100706, RRID:AB_312745
CD3e Monoclonal Antibody (145-2C11), PerCP-Cyanine5.5, eBioscience™	Invitrogen	Cat# 45-0031-82, RRID:AB_1107000
BV510 Rat Anti-Mouse CD45, 30-F11	BD Biosciences	Cat# *563891*, *RRID*:AB_2734134
APC Rat Anti-Mouse IFN-γ, XMG1.2	BD Biosciences	Cat# *554413*, *RRID*:AB_398551
PE-Cy™7 Rat Anti-Mouse TNF, MP6-XT22	BD Pharmingen	Cat# *557644*, *RRID*:AB_396761
PerCP/Cyanine5.5 anti-mouse CD8b (Ly-3) antibody, YTS156.7.7	BioLegend	Cat# 126609, RRID:AB_961304
PE/Cy7 anti-mouse CD69 antibody, H1.2F3	BioLegend	Cat# 104512, RRID:AB_493564
Pacific Blue™ anti-mouse CD3e antibody, 145-2C11	BioLegend	Cat# 100334, RRID:AB_2028475
APC/Fire™ 750 anti-mouse/human CD11b antibody, M1/70	BioLegend	Cat# 101262, RRID:AB_2572122
Biotin anti-mouse CD366 (Tim-3) antibody, RMT3-23	BioLegend	Cat# 119720, RRID:AB_2571936
Brilliant Violet 650™ Streptavidin	BioLegend	Cat# 405232
Brilliant Violet 785™ anti-mouse CD3e antibody, 145-2C11	BioLegend	Cat# 100355, RRID:AB_2565969
BV605 Rat Anti-Mouse CD45, 30-F11	BD Biosciences	Cat# *563053*, *RRID*:AB_2737976
BUV395 Rat Anti-Mouse CD44, IM7	BD Biosciences	Cat# *740215*, *RRID*:AB_2739963
BUV737 Rat Anti-Mouse CD8a, 53-6.7	BD Biosciences	Cat# *564297*, *RRID*:AB_2722580
FITC anti-mouse Ly-6C antibody, HK1.4	BioLegend	Cat# 128006, RRID:AB_1186135
PerCP/Cyanine5.5 anti-mouse CD24 antibody, M1/69	BioLegend	Cat# 101824, RRID:AB_1595491
Alexa Fluor® 647 Rat Anti-Mouse Siglec-F, E50-2440	BD Biosciences	Cat# *562680*, *RRID*:AB_2687570
Brilliant Violet 650™ anti-mouse F4/80 antibody, BM8	BioLegend	Cat# 123149, RRID:AB_2564589
Brilliant Violet 785™ anti-mouse I-A/I-E antibody, M5/114.15.2	BioLegend	Cat# 107645, RRID:AB_2565977
PE anti-mouse CD103 antibody, 2E7	BioLegend	Cat# 121406, RRID:AB_1133989
BUV395 Rat Anti-Mouse Ly-6G, 1A8	BD Biosciences	Cat# *563978*, *RRID*:AB_2716852
BUV737 Hamster Anti-Mouse CD11c, HL3	BD Biosciences	Cat# 564986, RRID:AB_2739034
FITC Rat Anti-Mouse CD44, IM7	BD Biosciences	Cat# 553133, RRID:AB_2076224
APC Hamster Anti-Mouse CD3e, 145-2C11	BD Biosciences	Cat# 553066, RRID:AB_398529
APC-Cy™7 Rat Anti-Mouse CD19, 1D3	BD Biosciences	Cat# 557655, RRID:AB_396770
Brilliant Violet 711™ anti-mouse CD25 antibody, PC61	BioLegend	Cat# 102049, RRID:AB_2564130
Brilliant Violet 785™ anti-mouse NK-1.1 antibody, PK136	BioLegend	Cat# 108749, RRID:AB_2564304
PE Rat Anti-Mouse CD62L, MEL-14	BD Biosciences	Cat# *553151*, *RRID*:AB_394666
BUV395 Rat Anti-Mouse CD8a, 53-6.7	*BD* Biosciences	Cat# *563786*, *RRID*:AB_2732919

BUV737 Rat Anti-Mouse CD4, RM4-5	*BD* Biosciences	Cat# *564933*, *RRID*:AB_2732918
FOXP3 Monoclonal Antibody (FJK-16s), PE, eBioscience™	Invitrogen	Cat# 12-5773-82, RRID:AB_465936
H-2D^{b} Adpgk Neoepitope Tetramer-ASMTNMELM-PE	MBL	Cat# TB-5113-1
H-2 Kb/KSFHFYCPL-APC	Immudex	Cat# JD4508-APC (this study)
H-2 Kb/ASIIVFNLL-APC	Immudex	Cat# JD4118-APC (this study)
InVivoMab anti-mouse PD-1 (CD279) antibody, RMP1-14	Bio X Cell	Cat# BE0146, RRID:AB_10949053
InVivoMab anti-mouse CTLA-4 (CD152) antibody, 9D9	Bio X Cell	Cat# BE0164, RRID:AB_10949609
Ultra-LEAF™ Purified anti-mouse CD40 antibody, 1C10	BioLegend	Cat# 102812, RRID:AB_2561489
LEAF™ Purified anti-mouse CD28 antibody, 37.51	BioLegend	Cat# 102112, RRID:AB_312877
Purified anti-mouse CD16/32 antibody, 93	BioLegend	Cat# 101302, RRID:AB_312801
Rat Anti-IFN-gamma Monoclonal Antibody, Unconjugated, Clone R4-6A2	BD Biosciences	Cat# 551216, RRID:AB_394094
Rat Anti-IFN-gamma Monoclonal Antibody, Biotin Conjugated, Clone XMG1.2	BD Biosciences	Cat# 554410, RRID:AB_395374
HRP Streptavidin for ELISPOT	BD Biosciences	Cat# 51-9000209
Biotin anti-mouse CD4 antibody, GK1.5	BioLegend	Cat# 100404, RRID:AB_312689
Biotin anti-mouse CD8a antibody, 53-6.7	BioLegend	Cat# 100704, RRID:AB_312743
Biotin anti-mouse/human CD45R/B220 antibody, RA3-6B2	BioLegend	Cat# 103204, RRID:AB_312989
Biotin anti-mouse I-Ab antibody, AF6-120.1	BioLegend	Cat# 116404, RRID:AB_313723
anti-mouse CD4 (GK1.5)	In Lab	N/A
anti-mouse CD8 (53-6.7)	In Lab	N/A
Chemicals, Peptides, and Recombinant Proteins		
H-2K^{b} MuLV p15E peptide	MBL	Cat# TS-M507-P
H-2D^{b} MutAdpgk Neoepitope ASMTNMELM synthetic peptide	GenScript	N/A (this study)
H-2K^{b} Neoepitope candidates and counterparts synthetic peptides	GenScript	N/A (this study)
LIVE/DEAD™ Fixable Violet Dead Cell Stain Kit, for 405 nm excitation	Invitrogen	Cat# L34964
LIVE/DEAD™ Fixable Aqua Dead Cell Stain Kit, for 405 nm excitation	Invitrogen	Cat# L34966
Collagenase D	Roche	Cat# 11088882001
DNase I	Roche	Cat# 11284932001
Poly(I:C)	TOCRIS	Cat# 4287
BD GolgiPlug™	BD Biosciences	Cat# 555029
Actinomycin D	Sigma	Cat# A1410
Polybrene Solution	Nacalai	Cat# 12996-81
FuGENE® 6 Transfection Reagent	Promega	Cat# E2691
Lipofectamine™ LTX Reagent with PLUS™ Reagent	ThermoFisher	Cat# 15338100
Critical Commercial Assays		
Mouse IFN-gamma DuoSet ELISA	R&D Systems	Cat# DY485-05
SMARTer® Mouse TCR a/b Profiling Kit	TAKARA BIO INC	Cat# Z4404N
Wizard® Genomic DNA Purification Kit	Promega	Cat# A1120
SureSelect XT Mouse All Exon	Agilent	Cat# 5190-4641
SureSelect Strand Specific RNA Reagent Kit	Agilent	Cat# G9691A
Agencourt AMPure XP Kit	Beckman Coulter Genomics	Cat# A63880
TRIzol™ LS Reagent	Invitrogen	Cat# 10296028
BD Cytofix/Cytoperm™	BD Biosciences	Cat# 554714
eBioscience™ Foxp3 / Transcription Factor Staining Buffer Set	Invitrogen	Cat# 00-5523-00
Premix WST-1 Cell Proliferation Assay System	Takara Bio	Cat# MK400
Deposited Data		
C57BL/6J blood Exome-Seq	DDBJ	DRA010264
MC38 WT or PD-L1 KO tumors Exome-Seq	DDBJ	DRA010264
MC38 WT or PD-L1 KO tumors RNA-Seq	DDBJ	DRA010264
TCR Seq for MutDpagt1 and MutCry1	DDBJ	DRA010264

Experimental Models: Cell Lines		
HEK293T	ATCC	Cat# CRL-3216
MC38	Dr. MT Lotze	N/A
EL4	ATCC	Cat# TIB-39
B16F10	ATCC	Cat# CRL-6475
E0771	CH3 BioSystems	Cat# 940001
TG40 mCD8A/mCD8B	Dr. Saito	N/A
Experimental Models: Organisms/Strains		
Mouse: C57BL/6	Charles River Japan	N/A
Mouse: Rag1(-/-)	The Jackson Laboratory	N/A
Recombinant DNA		
pMXs-IRES-GFP Retroviral Expression Vector	Cell Biolabs	Cat# RTV-013
pCas-Guide-EF1a-GFP CRISPR Vector	OriGene	Cat# GE100018
Software and Algorithms		
STAR	Dobin et al., 2013	https://github.com/alexdobin/STAR
NetMHCpan-3.0	Nielsen et al., 2016	http://tools.immuneepitope.org/mhci/
samtools v1.9	Li et al., 2009	http://www.htslib.org/download/
Picard Toolkit v2.20	Broad Institute	https://github.com/broadinstitute/picard
VarScan v2.4	Koboldt et al., 2012	http://dkoboldt.github.io/varscan/
bwa-mem2	Vasimuddin et al., 2019	https://github.com/bwa-mem2/bwa-mem2
bwa v0.7	Li et al., 2009	http://bio-bwa.sourceforge.net/
GATK v3	Broad Institute	https://software.broadinstitute.org/gatk/
ClicO FS	Cheong et al., 2015	clicofs.codoncloud.com
R3.6.1	The R Project	https://www.r-project.org/
RStudio Desktop	RStudio Team	https://rstudio.com/
TCGAbiolinksGUI	Silva et al., 2018	https://bioconductor.org/packages/release/bioc/html/TCGAbiolinksGUI.html
gdc-rnaseq-tool	Dr. Reid	https://github.com/cpreid2/gdc-rnaseq-tool
FlowJo v10.5.3	BD	https://www.flowjo.com/
FlowJo plugins FlowSOM v1.5	Gassen et al., 2015	https://www.flowjo.com/exchange/#/
Excel	Microsoft	https://products.office.com/ja-jp/excel
StatMate V for Win&Mac Hybrid	ATMS Co.,Ltd	http://atms-shop.jp/?pid=64906245
LymAnalyzer_gui v1.2.2	Yu et al., 2016	https://sourceforge.net/projects/lymanalyzer/
TCRdist v0.0.2	Dash et al., 2017	https://github.com/phbradley/tcr-dist
SeqKit v0.8	Shen et al., 2016	https://bioinf.shenwei.me/seqkit/
signeR	Rosales RA et al., 2016	https://bioconductor.org/packages/release/bioc/html/signeR.html

References

Dash, P., Fiore-Gartland, A.J., Hertz, T., Wang, G.C., Sharma, S., Souquette, A., Crawford, J.C., Clemens, E.B., Nguyen, T.H.O., Kedzierska, K., et al. (2017). Quantifiable predictive features define epitope-specific T cell receptor repertoires. Nature *547*, 89-93.

Dobin, A., Davis, C.A., Schlesinger, F., Drenkow, J., Zaleski, C., Jha, S., Batut, P., Chaisson, M. and Gingeras, T.R. (2013). STAR: ultrafast universal RNA-seq aligner. Bioinformatics *29*, 15-21.

Koboldt, D.C., Zhang, Q., Larson, D.E., Shen, D., McLellan, M.D., Lin, L., Miller, C.A., Mardis, E.R., Ding, L. and Wilson, R.K. (2012). VarScan 2: somatic mutation and copy number alteration discovery in cancer by exome sequencing. Genome Res *22*, 568-576.

Li, H. (2011). A statistical framework for SNP calling, mutation discovery, association mapping and population genetical parameter estimation from sequencing data. Bioinformatics *27*, 2987-2993.

Li, H. (2013). Aligning sequence reads, clone sequences and assembly contigs with BWA-MEM. arXiv preprint arXiv:1303.3997.

Li, H., Handsaker, B., Wysoker, A., Fennell, T., Ruan, J., Homer, N., Marth, G., Abecasis, G., Durbin, R. and Genome Project Data Processing, S. (2009). The Sequence Alignment/Map format and SAMtools. Bioinformatics *25*, 2078-2079.

McKenna, A., Hanna, M., Banks, E., Sivachenko, A., Cibulskis, K., Kernytsky, A., Garimella, K., Altshuler, D., Gabriel, S., Daly, M., et al. (2010). The Genome Analysis Toolkit: a MapReduce framework for analyzing next-generation DNA sequencing data. Genome Res *20*, 1297-1303.

Nielsen, M. and Andreatta, M. (2016). NetMHCpan-3.0; improved prediction of binding to MHC class I molecules integrating information from multiple receptor and peptide length datasets. Genome Med *8*, 33.

Shen, W., Le, S., Li, Y. and Hu, F. (2016). SeqKit: A Cross-Platform and Ultrafast Toolkit for FASTA/Q File Manipulation. PLoS One *11*, e0163962.

Shimizu, K. and Fujii, S. (2009). DC therapy induces long-term NK reactivity to tumors via host DC. Eur J Immunol *39*, 457-468.

Shimizu, K., Hidaka, M., Kadowaki, N., Makita, N., Konishi, N., Fujimoto, K., Uchiyama, T., Kawano, F., Taniguchi, M. and Fujii, S. (2006). Evaluation of the function of human invariant NKT cells from cancer patients using α-galactosylceramide-loaded murine dendritic cells. J. Immunol. *177*, 3484-3492.

Shimizu, K., Kurosawa, Y., Taniguchi, M., Steinman, R.M. and Fujii, S. (2007). Cross-presentation of glycolipid from tumor cells loaded with α-galactosylceramide leads to potent and long-lived T cell mediated immunity via dendritic cells. J. Exp. Med. *204*, 2641-2653.

Silva, T.C., Colaprico, A., Olsen, C., Malta, T.M., Bontempi, G., Ceccarelli, M., Berman, B.P. and Noushmehr, H. (2018). Tcgabiolinksgui: a graphical user interface to analyze cancer molecular and clinical data. F1000Research *7*.

Vasimuddin, M., Misra, S., Li, H. and Aluru, S. (2019) Efficient architecture-aware acceleration of BWA-MEM for multicore systems: IEEE. pp. 314-324.

Yokosuka, T., Takase, K., Suzuki, M., Nakagawa, Y., Taki, S., Takahashi, H., Fujisawa, T., Arase, H. and Saito, T. (2002). Predominant role of T cell receptor (TCR)-alpha chain in forming preimmune TCR repertoire revealed by clonal TCR reconstitution system. J Exp Med *195*, 991-1001.

Yu, Y., Ceredig, R. and Seoighe, C. (2016). LymAnalyzer: a tool for comprehensive analysis of next generation sequencing data of T cell receptors and immunoglobulins. Nucleic Acids Res *44*, e31.